Remote Sensing of Environment 144 (2014) 197–213

Contents lists available at ScienceDirect

Remote Sensing of Environment

journal homepage: www.elsevier.com/locate/rse

Remote monitoring of soil moisture using passive microwave-based techniques — Theoretical basis and overview of selected algorithms for AMSR-E

I.E. Mladenova [a,*], T.J. Jackson [a], E. Njoku [b], R. Bindlish [c], S. Chan [b], M.H. Cosh [a], T.R.H. Holmes [a], R.A.M. de Jeu [d], L. Jones [e,f], J. Kimball [e,f], S. Paloscia [g], E. Santi [g]

[a] USDA, Hydrology and Remote Sensing Lab, Beltsville, MD 20705, USA
[b] Jet Propulsion Laboratory, California Institute of Technology, Pasadena, CA 91109, USA
[c] Science System and Applications Inc., Lanham, MD 20706, USA
[d] VU University Amsterdam, Faculty of Earth and Life Sciences, Amsterdam, The Netherlands
[e] The University of Montana, Flathead Lake Biological Station, Polson, MT 59860, USA
[f] The University of Montana, Numerical Terradynamic Simulation Group, Missoula, MT 59812, USA
[g] National Research Council, Institute of Applied Physics, Florence, Italy

ARTICLE INFO

Article history:
Received 10 April 2013
Received in revised form 15 January 2014
Accepted 18 January 2014
Available online 20 February 2014

Keywords:
Soil moisture
Algorithms
Passive microwave
Radiative transfer modeling
Forward/inverse modeling
AMSR-E

ABSTRACT

Satellite-based passive microwave remote sensing has been shown to be a valuable tool in mapping and monitoring global soil moisture. The Advanced Microwave Scanning Radiometer on the Aqua platform (AMSR-E) has made significant contributions to this application. As the result of agency and individual initiatives, several approaches for the retrieval of soil moisture from AMSR-E have been proposed and implemented. Although the majority of these are based on the same Radiative Transfer Equation, studies have shown that the resulting soil moisture estimates can differ significantly. A primary goal of this investigation is to understand these differences and develop a suitable approach to potentially improve the algorithm currently used by NASA in producing its operational soil moisture product. In order to achieve this goal, the theoretical basis of several alternative soil moisture retrieval algorithms are examined. Analysis has focused on five established approaches: the operational algorithm adopted by NASA, which is referred to as the Normalized Polarization Difference algorithm, the Single Channel Algorithm, the Land Parameter Retrieval Model, the University of Montana soil moisture algorithm, and the HydroAlgo Artificial Neural Network algorithm. Previous comparisons of these algorithms in the literature have typically focused on the retrieved soil moisture products, and employed different metrics and data sets, and have resulted in differing conclusions. In this investigation we attempt to provide a more thorough understanding of the fundamental differences between the algorithms and how these differences affect their performance in terms of range of soil moisture provided. The comparative overview presented in the paper is based on the operating versions of the source codes of the individual algorithms. Analysis has indicated that the differences between algorithms lie in the specific parameterizations and assumptions of each algorithm. The comparative overview of the theoretical basis of the approaches is linked to differences found in the soil moisture retrievals, leading to suggestions for improvements and increased reliability in these algorithms.

Published by Elsevier Inc.

1. Introduction

Global soil moisture (*SM*) is an important component of the terrestrial water cycle. The acceptance and integration of *SM* in models and decision processes have been in part the result of the availability of satellite-based products derived using microwave remote sensing (Bolten et al., 2010; Drusch, 2007). Depending on the source of energy, microwave remote sensing techniques can be grouped in two categories: active (radar/backscatter)-based and passive (radiometer/brightness temperature)-based. Here we will be concerned only with passive microwave remote sensing.

The soil moisture information provided by passive microwave remote sensing lies in the complex atmosphere–land (surface/sub-surface)-system interactions described by a Radiative Transfer Equation (RTE) (Kerr and Njoku, 1990; Ulaby et al., 1986). Implementation of this model requires characterizing the components of the geo-/bio-physical system and providing parameters that may be dependent on the system configuration. If all of these factors are considered to be significant and incorporated into the algorithm, this can result in an under-determined system of equations (i.e., more

* Corresponding author at: USDA-ARS, Hydrology and Remote Sensing Lab, BARC-West, B007, 10300 Baltimore Ave., Beltsville, MD 20705, USA. Tel.: +1 301 504 9109.
E-mail address: Iliana.Mladenova@ARS.USDA.GOV (I.E. Mladenova).

0034-4257/$ – see front matter. Published by Elsevier Inc.
http://dx.doi.org/10.1016/j.rse.2014.01.013

unknowns than measurements), regardless of how many frequencies and polarizations are available. Implementing theory into a practical soil moisture retrieval algorithm requires a reduction in the dimensionality by making simplifying assumptions or providing a priori estimates of some parameters (ancillary data). Different algorithms have evolved based upon how the developers have dealt with the dimensionality and the characteristics of the observing system.

One of the most important factors influencing the proliferation of satellite-based soil moisture mapping has been the Advanced Microwave Scanning Radiometer on NASA's Earth Observing System Aqua satellite (AMSR-E, http://www.ghcc.msfc.nasa.gov/AMSR/). AMSR-E has provided a 10-year data record that is now being extended by the recently launched AMSR2 instrument on the Japanese Aerospace Exploration Agency (JAXA) Global Climate Observing Mission-Water satellite (GCOM-W, http://www.jaxa.jp/projects/sat/gcom_w/index_e.html), potentially leading to a consistent long-term climate data record obtained from the same instrument. The availability of such a long-term global data record will benefit research studies that require information on long-term soil moisture trends.

Both NASA and JAXA have supported development of standard soil moisture products (Kawanishi et al., 2003; Shibata et al., 2003). Research studies that have used the NASA AMSR-E standard soil moisture products available from the National Snow and Ice Data Center (NSIDC; http://nsidc.org/data/ae_land.html) have noted performance issues with the NASA standard products derived using the Normalized Polarization Difference algorithm developed by Njoku and Chan (2006), specifically a narrow dynamic range and inadequate temporal response of the soil moisture retrievals (Draper et al., 2009; Jackson et al., 2010), where the later is considered to be the most important indicator of the skill of soil moisture product (Koster et al., 2009; Reichle et al., 2004). In this study our goal was to investigate the sensitivity of the NPD algorithm, to define its temporal dynamics through intercomparisons with other established soil moisture algorithms, and to explore whether the algorithm performance can be improved by implementing elements of other more recently established soil moisture algorithms.

In approaching the problem, we limited our scope to using well-established algorithms that have been peer-reviewed and implemented at some level by an operational or data providing agency. In addition, we stipulated that all algorithms should be capable of being applied globally (subject to flags) and be capable of operating in a stand-alone mode, i.e., independently of externally-provided dynamic ancillary data. As noted above, our motivation for this investigation was to gain a better understating of the NPD algorithm data product distributed through the NSIDC (http://nsidc.org/data/amsre/), which uses as input NASA AMSR-E Level 2A data (calibrated brightness temperatures, T_B). Within this context, we focus on approaches that are capable of soil moisture retrieval using the same AMSR-E-based data set as employed by the NPD algorithm. It should be noted that JAXA utilizes its own AMSR-E Level 1 data to produce a soil moisture product. Differences in the calibration processing of the two data sets complicate direct intercomparisons. Therefore, we did not include the JAXA standard product/algorithm in this investigation and cannot make any direct conclusions on its comparative performance with the other algorithms. The analysis presented here is based not only on the published literature but also expands on this with information extracted from the algorithms' source codes and communications with algorithm developers.

The following five approaches were examined:

(1) Normalized Polarization Difference (NPD) algorithm,
(2) Single Channel Algorithm (SCA),
(3) Land Parameter Retrieval Model (LPRM),
(4) University of Montana (UMT) land surface retrieval algorithm,
(5) HydroAlgo Artificial Neural Network-based (HA-ANN) algorithm

All these algorithms are in principle based on the same RTE (Table 1).

Total T_B as measured by the satellite at the top of the atmosphere includes information on all intervening constituents within the satellite sensor viewing path. The total microwave signal is expressed as an integrated measure of several inter-related components that describe the three major contributing layers; atmosphere, vegetation and soil. Overall, the general data flow and retrieval logic implemented by all algorithms considered here are similar. Implementing soil moisture retrieval requires that the attenuating components, i.e. atmospheric water vapor, vegetation, roughness, etc., are correctly accounted for. As discussed later, there are various ways to do this.

This study is not meant as a quantitative inter-comparison; several of these have been presented in the literature (Crow et al., 2010; Draper et al., 2009; Jackson et al., 2010). Instead, this paper offers an in-depth conceptual discussion focused on the theoretical background of the suite of algorithms selected, and attempts to present them in parallel. We will be attempting to understand how the basic premises of the algorithms impact their performance in terms of the range of soil moisture provided. The approach followed in this paper is to: (1) present a comparative overview of the theoretical bases of available passive-based approaches that are compatible with AMSR-E (based upon our specified filters); (2) outline differences and clarify their importance to the sensitivity of the final *SM* estimates; and (3) address the option of possible transferability in terms of theoretical components (i.e. atmospheric correction, vegetation/roughness modeling, etc.) between the approaches. Potential outcomes of the current study include gaining a better understanding of the available retrieval approaches, identifying causes of the observed differences between the retrievals, and providing guidelines for reprocessing of the archived AMSR-E soil moisture data using a modification or upgrade of the NPD algorithm. Furthermore, the analyses may provide valuable algorithm feedback for other soil moisture missions such as GCOM-W (Imaoka et al., 2010; Oki et al., 2010), Soil Moisture Ocean Salinity (SMOS; Kerr et al., 2012), and Soil Moisture Active Passive (SMAP; Entekhabi et al., 2010).

The paper is structured as follows: Section 2 is composed of two parts that provide a historic overview and introduce the common background of the currently available techniques. The specific components pertinent to each individual approach are then discussed separately for each algorithm in Section 3. Section 4 aims at providing a comparative theoretical overview of the algorithm-specific RTE solutions, as well

Table 1
Algorithm overview table.

Algorithm		Agency	Reference
1	Normalized Polarization Difference algorithm: NPD	National Aeronautics Space Administration, USA	Njoku and Chan (2006)
2	Single Channel Algorithm: SCA	U.S. Department of Agriculture, USA	Jackson (1993)
3	Land Parameter Retrieval Model: LPRM	Free University of Amsterdam, the Netherlands	Owe et al. (2001), De Jeu and Owe (2003)
4	Land surface retrieval algorithm: UMT	University of Montana, USA	Jones et al. (2009), Jones et al.(2011)
5	HydroAlgo Artificial Neural Network algorithm HA-ANN	National Research Council, Nello Carrara Institute of Applied Physics, Italy	Santi et al. (2012)

as the key biophysical components and the approaches used for their estimation. The major highlights are then summarized in Section 5.

2. Algorithm theoretical basis

2.1. Timeline and motivation

Developments in the area of passive microwave remote sensing of *SM* have gone through three major stages: (I) acquiring a general theoretical knowledge and basic understanding of the microwave signal and its relation to land surface variables and processes, (II) establishing theoretically-based soil moisture retrieval algorithms for application to airborne or spaceborne observational data, and (III) global operational implementations.

Beginning in the 1970s and continuing to some degree up to the early 1990s, efforts were concentrated on developing, verifying and improving the basic microwave emission models for smooth and rough soils (i.e. Mo et al., 1982; Stogryn, 1970; Ulaby et al., 1986; Wilheit, 1978) and soil–water dielectric mixing models (i.e. Dobson et al., 1985; Hallikainen et al., 1985; Jackson et al., 1982; Wang and Schmugge, 1980). These efforts provided the linkage between T_B and *SM*.

In parallel with these early modeling efforts, controlled condition field campaigns were conducted in order to provide suitable datasets for understanding and expanding the basic emissivity–soil moisture relationship, in particular for vegetated conditions (i.e. Ferrazzoli et al., 1992; Lee, 1974; Paloscia et al., 1993; Poe and Edgerton, 1971; Wang et al., 1982). These experiments focused on exploring the sensitivity of the measured microwave emission to changes in the sensor system characteristics (i.e., frequency, polarization, angular geometry) and ground conditions (i.e., vegetation, roughness, soil wetness and texture, physical temperature, etc.). From these investigations, baseline approaches to account for three major variables; physical temperature, roughness and vegetation, were developed (i.e. Choudhury et al., 1979; Jackson and Schmugge, 1991; Kirdiashev et al., 1979; Mo and Schmugge, 1987; Wang and Choudhury, 1981). These advances resulted in the form of the RTE that has been applied to vegetative conditions (the τ–ω model; Mo et al., 1982), which serves as the basis for almost all retrieval algorithms.

The above research also defined the benefits of using low frequency (<11 GHz) passive microwave observations for routine and large scale soil moisture mapping. However, operational efforts have been constrained by antenna technology and the availability of suitable radiometer systems in space. Data collection using space-borne microwave radiometers dates back to the early 1960s (see Chapter 14 and Table 14.1 in Sharkov, 2003). These data include the S-194 microwave sensor that operated on Skylab in the 1970s (http://www.eoportal.org/directory/pres_SkylabSpaceStation.html), which incorporated the optimal frequency (1.4 GHz) for surface soil moisture retrieval, but provided observations with very limited temporal and spatial coverage and low resolution (Jackson et al., 2004). Another low frequency-instrument was the Scanning Multichannel Microwave Radiometer (SMMR, http://nsidc.org/daac/projects/passivemicro/smmr.html) on Nimbus 7 that collected multi-frequency (6.6, 10.7, 18.0 and 37.0 GHz) data at low resolution (150 km for C-band). Additional operationally oriented satellite microwave sensors with limited potential for soil moisture retrieval include the Special Sensor Microwave/Imager (SSM/I, http://nsidc.org/data/docs/daac/ssmi_instrument.gd.html) carried aboard the Defense Meteorological Satellite Program (DMSP) satellites (1987–present), which has good temporal coverage but a suboptimal frequency range (>19.3 GHz). The Tropical Rainfall Measuring Mission's (TRMM) Microwave Imager (TMI, http://trmm.gsfc.nasa.gov/overview_dir/tmi.html) is another operational system that includes a 10.6 GHz channel with approximately 50 km spatial resolution, but only covers a limited latitude range (38°N–38°S).

Stage II was aided by the publication of the first complete RTE-based algorithm that allowed direct T_B–*SM* inversion (Jackson and Schmugge, 1989), which is referred to as the Single Channel Algorithm (SCA). This approach was developed initially to support the relatively simple instrument configurations that were available on aircraft platforms. In this approach the soil moisture contribution is estimated by sequentially performing temperature normalization, removing the attenuating effects of the overlaying vegetation and atmosphere, and estimating the associated smooth (i.e. removed the surface roughness effects) surface emissivity using ancillary data. The Fresnel equation is used to convert the emissivity to a dielectric constant and then the resulting estimate of the dielectric constant is linked to soil moisture using a dielectric mixing model. The SCA will be discussed in more detail later in the paper.

With AMSR-E on the horizon, Njoku and Li (1999) proposed an algorithm that would attempt to utilize all of the lowest three frequency channels of the instrument (C, X, and Ka) in an iterative optimization scheme to simultaneously solve the RTE for soil moisture, vegetation water content and surface temperature. Other multichannel AMSR-E algorithms were also developed subsequently as discussed below.

Stage III began in the late 1990s with the preparation for launch of AMSR-E in 2002 (as well as the short-lived AMSR). This instrument brought together several important design features; global coverage, moderate spatial resolution, multi-frequency passive microwave observations that included low frequencies, and publicly available data provided in a timely manner. It was designed to satisfy retrieval of a wide range of geophysical variables, which for the first time included an operational soil moisture product (Kawanishi et al., 2003; Shibata et al., 2003). Both NASA and JAXA supported the implementation of soil moisture as a standard product but took somewhat different approaches to selecting an algorithm. NASA solicited proposals and selected a single team/algorithm for a specific set of products. The original version of the *SM* algorithm was described in Njoku and Li (1999) and Njoku et al. (2003). This was later modified significantly to include elements described in Njoku and Chan (2006) and is referred to as the Normalized Polarization Difference algorithm.

JAXA on the other hand solicited proposals and identified four alternative methods as research algorithms (including the original Njoku and Li (1999) algorithm). Over a period of several years, these algorithms were evaluated by benchmarking against common in situ datasets, before selecting the algorithm described in Koike et al. (2004) and Lu et al. (2009) as the JAXA standard algorithm. In addition, JAXA offered continued support to the other approaches as research algorithms, including the Single Channel Algorithm (Jackson, 1993) and a retrieval approach developed by Paloscia et al. (2001) and Paloscia et al. (2006).

The routine availability of AMSR-E T_B data stimulated later development and evolution of several other algorithm approaches leading to the LPRM (De Jeu and Owe, 2003; Owe et al. 2001), UMT (Jones et al., 2009, 2010), and HA-ANN (Santi et al., 2012) soil moisture products.

The algorithms presented and discussed here have several common components: all

(1) are based on the same RTE formulation and utilize the τ–ω model of Mo et al. (1982) to represent the electromagnetic radiation from the Earth's surface;
(2) correct for the vegetation and roughness effects;
(3) assume horizontal homogeneity over the land portion of the satellite footprint and ignore the vertical variability within the atmospheric, vegetation and soil layers;
(4) assume that effective temperature of the emitting soil and the overlying vegetation layer are approximately the same, i.e. $T^c \cong T^s$;
(5) utilize the Fresnel equations to relate the microwave reflectivity to the dielectric properties of the soil;
(6) rely on soil texture data as an ancillary input, necessary for the

inversion from dielectric constant to soil moisture;

(7) do not attempt retrieval over RFI contaminated areas, frozen soils, densely vegetated and snow-covered areas, and open water.

HA-ANN uses artificial neural network-based training for *SM* estimation, which relies on field-collected *SM* measurements concurrent with T_B observations. The T_B data set includes both actual and simulated brightness temperature data, where the latter are generated using RTE modeling. Therefore, the above listed similarities are also relevant to the HA-ANN algorithm.

Items (6) and (7) typically involve the use of ancillary data sets or threshold-based techniques, which generally vary with the algorithms. Some of the commonly used ancillary data sets include soil texture and land cover information. Details on the algorithm specific data sets used will be introduced when discussing the individual approaches. Ancillary data sets have two roles in these algorithms: providing input for the actual retrieval and as information for identifying areas where the retrieval is not feasible (flags), i.e. open water bodies, frozen soils, etc. Along with the choice of the ancillary data set there are several related factors that also need to be considered: the land cover classification scheme and any gridding or post-processing techniques involved. For example, it should be noted that, in general, the data sets employed by the individual approaches do not have the same native spatial resolution as AMSR-E. The desired land information may be extracted or the data may be gridded using different sampling logic (i.e. land cover type/ground conditions: nearest distance vs. the dominant type; soil characteristics: nearest distance vs. average; swath to grid conversion: last drop in the bucket vs. linear averaging). The choice of post-processing logic can introduce differences in terms of ground conditions used in the individual retrievals for the same location.

Before discussing the actual equations, the annotation logic adopted in this paper is introduced. This attempts to resolve the different terminology and symbols used by the different algorithms. System-related parameters are shown as subscripts (i.e. Table 2.2), while any other characteristic used to describe ground conditions or specify emitting media are shown as superscripts (i.e. Table 2.3). Please refer to Table 2 for a full list of symbols/abbreviations.

2.2. General background

The overall retrieval process, shown schematically in Fig. 1, includes two major components: modeling the thermal radiation from the earth surface using radiative transfer theory and applying a dielectric mixing model to estimate *SM*. These two elements are related through the Fresnel reflectivity model (Eqs. 1a and 1b).

$$R^{smooth}_{(f,H)} = \left|\frac{\cos\theta - \left(\kappa - \sin^2\theta\right)^{0.5}}{\cos\theta + \left(\kappa - \sin^2\theta\right)^{0.5}}\right|^2 \tag{1a}$$

$$R^{smooth}_{(f,V)} = \left|\frac{\kappa\cos\theta - \left(\kappa - \sin^2\theta\right)^{0.5}}{\kappa\cos\theta + \left(\kappa - \sin^2\theta\right)^{0.5}}\right|^2 . \tag{1b}$$

For a specific frequency (f), the smooth soil reflectivity (R), is a function of polarization ($p = H$ or V), where H or V indicates horizontal or vertical polarization, respectively, incidence angle (θ), and complex dielectric constant of the soil–water mixture (κ). κ is dependent upon the water content. The real part of the dielectric constant κ' describes the propagation characteristics of the energy through the soil, while κ'' characterizes the energy loss in the soil. At the low frequency range considered here κ'' is relatively small compared to κ' (Dobson et al., 1985; Hallikainen et al., 1985; Wang and Schmugge, 1980). By low frequency range in this paper we mean $f \leq 11$ GHz, which includes the two lowest AMSR-E frequencies 6.9 and 10.7 GHz. Since we are concerned here only with AMSR-E, which is a constant incidence angle (θ) system, the θ dependence will be omitted from further equations for simplicity.

The surface reflectivity $R_{(f,\,p)}$ at microwave frequencies is related to the emissivity $e_{(f,\,p)}$ by: $R_{(f,\,p)} = 1 - e_{(f,\,p)}$. The emissivity is derived from the radiative transfer model:

$$T^{t}_{B(f,p)} = T^{a\uparrow}_{B(f,p)} + e^{-\tau^{a}_{(f,p)}}\left(1 - e^{rough}_{(f,p)}\right)\left(T^{a\downarrow}_{B(f,p)} + e^{-\tau^{a}_{(f,p)}}T^{sky}_{B}\right) + e^{-\tau^{a}_{(f,p)}}T^{l}_{B(f,p)}, \tag{2}$$

Table 2
Symbols, annotation and abbreviations.

Parameter	Symbol
1. Modeling	
T_B	Brightness temperature
T	Effective/physical temperature
SM	Soil moisture
$\kappa('/'')$	(Real/imaginary) part of the complex dielectric constant of the soil–water mixture
R	Reflectivity
e	Emissivity
Γ	Transmissivity
τ	Optical depth
ω	Single scattering albedo
g	Vegetation–roughness parameter
a	Frequency dependent proportionality constant
ts	Current ground conditions
h, Q	Roughness parameters
b	Vegetation parameter
MOD/OBS	MODeled/OBServed
F( ) or ( )	Function of ( )
$C^{\#}, \beta^{\#}, x^{\#}, a^{\#}, b^{\#}$	Model coefficients (# = 0, 1, 2, …)
2. System	
p	Polarization
H	Horizontal polarization
V	Vertical polarization
f	Frequency
θ	Incidence angle
3. Terrain/media	
rough	Rough surface conditions
smooth	Smooth surface conditions
effective	Effective physical temperature
composite	Composite surface emissivity (UMT)
t	Total
l	Land
s	Soil
a	Atmosphere
c	Canopy/vegetation
w	Water
ice, rock, air	Ice, rock, air
dry	Dry soil moisture conditions
β_d	Soil bulk density
4. Ratios/indices	
NDVI	Normalized Difference Vegetation Index
NPD	Normalized Polarization Difference
MPDI	Microwave Polarization Difference Index
MAWVI	Microwave Atmospheric Water Vapor Index
V	Vertical Atmospheric Water vapor Content
VWC	Vegetation Water Content
a	Slope of the land–water emissivity ratio (UMT)
FI	Frequency Index
PR	Polarization ratio
5. Other	
AMSR-E	Advanced Microwave Scanning Radiometer
SMOS	Soil Moisture Ocean Salinity
SMAP	Soil Moisture Active Passive
AVHRR	Advanced Very high Resolution Radiometer
MODIS	MODerate resolution Imaging Spectroradiometer
UMD	University of Maryland land cover classification scheme
IGBP	International Geosphere–Biosphere Programme
GLDAS	Global Land Data Assimilation System data products
FNOC	US Naval Fleet Numerical Oceanographic Center
ATBD	Algorithm Theoretical Basis Documents

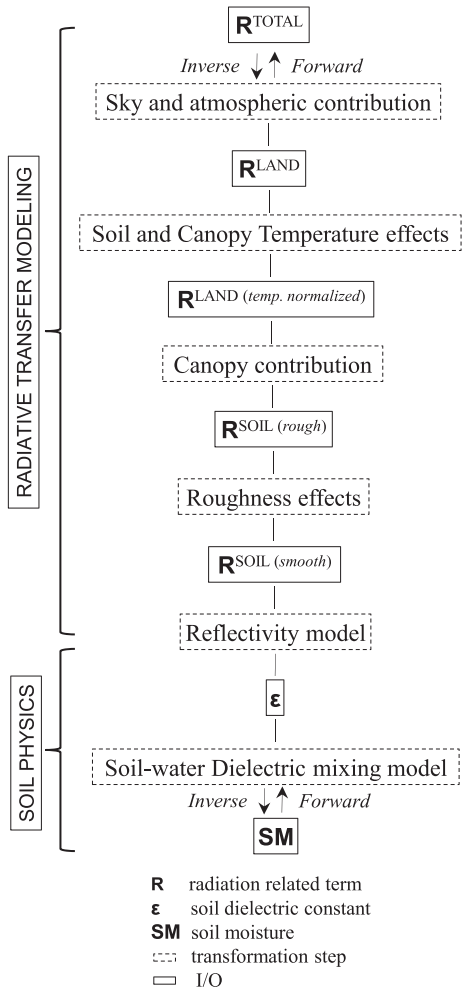

Fig. 1. Schematic representation of a passive-based soil moisture retrieval model. Shown here is the general data flow of both forward and inverse modeling. Solutions are based on solving the radiative transfer set of equations and estimating the soil water content through using a soil–water dielectric model.

where $T_B^t(f, p)$ indicates the total brightness temperature as measured by the satellite, often called top of atmosphere brightness temperature, $T_B^l(f, p)$ is the brightness temperature of the land, $T_{B(f,p)}^{a\uparrow/\downarrow}$ and T_B^{sky} stand for up-/down-welling atmospheric and sky temperatures, respectively, and $e_{(f,\ p)}{}^{rough}$ is the emissivity of rough soil. The attenuating effects of the atmosphere is accounted for by the opacity terms $\tau_{(f,\ p)}{}^{a}$, which refer to the opacity along the slant path through the atmosphere.

An explanation of Eq. (2) is given by Kerr and Njoku (1990). The first term is the atmospheric emission that propagates upwards directly towards the radiometer system. The second term is the sum of the atmospherically attenuated cosmic background emission and the downward atmospheric emission, which is reflected at the land surface and then attenuated by the atmosphere. The last term summarizes the atmospherically attenuated upwelling radiation emitted by the land surface ($T_B^l(f, p)$).

The magnitude of the atmospheric contribution varies with frequency. At the low microwave frequencies used for retrieval of soil moisture (i.e. L-, C- and X-band) the atmospheric contribution is negligible relative to $T_B^l(f, p)$ and, most importantly, the atmospheric opacity ($\tau^a(f, p)$) is very low (Ulaby et al., 1986). Thus, for soil moisture retrieval the atmosphere can be well approximated as a transparent layer (Jackson, 1993), in which case $T_{B(f,p)}^t \cong T_{B(f,p)}^l$.

The complete formulation of $T_B^l(f, p)$ is given by Mo et al. (1982) and is known as the τ–ω model

$$T_{B(f,p)}^l = T^s e_{(f,p)}^{rough} e^{-\tau_{(f,p)}^c} + T^c\left(1-\omega_{(f,p)}\right)\left(1-e^{-\tau_{(f,p)}^c}\right) + e^{-\tau_{(f,p)}^c} T^c\left(1-\omega_{(f,p)}\right)\left(1-e^{-\tau_{(f,p)}^c}\right)\left(1-e_{(f,p)}^{rough}\right), \quad (3)$$

where $\tau_{(f,\ p)}{}^c$ is vegetation optical depth, $\omega_{(f,p)}$ is the single scattering albedo, and T^c and T^s are the physical temperatures of the vegetation and the soil layers, respectively.

Eq. (3) shows that the total upward land radiation is composed of three terms: direct upward soil radiation attenuated by the vegetation, direct upward canopy radiation, and downward canopy radiation. As with the atmospheric radiation, the radiation emitted by the canopy can be both upward (second term of Eq. 3) and downward towards the soil surface, where the latter is reflected backward towards the radiometer and attenuated again by the canopy (third term of Eq. 3). The τ–ω model ignores multiple scattering within the vegetation layer, which is considered a reasonable assumption at the (low) frequency range used for soil moisture sensing.

In Eq. (3) the soil and vegetation media are modeled as homogeneous layers with temperatures T^s and T^c, respectively. When the media characteristics are non-uniform over the radiative emission depths the temperatures and emissivities in Eq. (3) are considered as "effective" parameters (weighted averages over the emission paths). In the context of passive-based retrieval of soil moisture, the soil and vegetation continuum is modeled as continuous uniform layers that have been assumed to have equal temperatures (i.e. $T^s \cong T^c$).

The relationship between rough and smooth surface reflectivity can be modeled using the h–Q formulation described by Wang et al. (1983)

$$R_{(f,H)}^{s,rough} = \left[\left(1-Q_{(f)}\right)R_{(f,H)}^{s,smooth} + Q_{(f)}R_{(f,V)}^{s,smooth}\right]e^{-G(\theta)h_{(f)}}, \quad (4a)$$

and

$$R_{(f,V)}^{s,rough} = \left[\left(1-Q_{(f)}\right)R_{(f,V)}^{s,smooth} + Q_{(f)}R_{(f,H)}^{s,smooth}\right]e^{-G(\theta)h_{(f)}}. \quad (4b)$$

$h_{(f)}$ and $Q_{(f)}$ are parameters related to the surface root mean square (RMS) height and horizontal roughness correlation length, and $G(\theta) \cong 1$, where G is generally a function dependent on incidence angle. Eq. (4) is an extension of an earlier roughness model developed by Choudhury et al. (1979), which is equivalent to Eqs. (4a) and (4b) with $Q_{(f)} = 0$ and $G(\theta) = \cos{}^2\theta$.

The vegetation attenuation effect in the τ–ω model is represented by the $\omega_{(f,p)}$ and $\tau_{(f,p)}^c$ parameters, which are dependent on vegetation water content and structure, incidence angle, frequency and polarization (Van De Griend and Wigneron, 2004). Confirmation of the $\omega_{(f,p)}$ and $\tau_{(f,p)}^c$ dependence on polarization in the literature is limited. Some of the past experiments have demonstrated minimal variability in vegetation attenuation properties between H- and V-pol over agricultural fields, where the individual plant constituents had a distinct preferential orientation (Ulaby et al., 1986; Van De Griend and Owe, 1994). Consequently, in approaches that use dual-polarizations or polarization-based indices (i.e. NPD LPRM, UMT) it is assumed that $\omega_{(f,H)} = \omega_{(f,V)}$ and $\tau_{(f,H)}^c = \tau_{(f,V)}^c$. This assumption results in simplification of the $\omega_{(f)}$ and $\tau_{(f)}^c$ expressions.

The single scattering albedo accounts for the canopy volume scattering and total extinction properties and is expressed as the ratio of these two quantities (Mo et al., 1982; Ulaby and Wilson, 1985; Ulaby et al., 1986). However, there is limited information on the temporal or canopy type variability of this parameter. All of the algorithm approaches considered here use a constant global value. Overall, the reported $\omega_{(f)}$ values are generally small ($0.04 < \omega_{(f)} < 0.12$; Jackson and O'Neill, 1991; Van De Griend and Owe, 1994). As summarized by Van De Griend and Owe, (1994) $\omega_{(f)}$ has a minimal/negligible effect on the

range of the emitted radiation from vegetated surfaces at microwave wavelengths.

If we use the simplifying assumptions discussed above, where $T^s \cong T^c$ and $\omega_{(f)} = 0$, we obtain the following important simplification of Eq. (3), i.e.

$$T^l_{B(f,p)} = T^s\left(1 - R^{rough}_{(f,p)} e^{-2\tau^c_{(f,p)}}\right). \tag{5}$$

Among all the parameters that impact soil moisture retrieval, vegetation water content (*VWC*) is the most significant (Jackson and Schmugge, 1991). The vegetation opacity $\tau^c_{(f)}$ is governed by the thickness of the vegetation layer and its extinction properties, which in turn are functionally related to the *VWC* and depend also on the type of vegetation and its structure. Thus, the vegetation opacity is expected to have significant temporal and spatial variability.

The vegetation opacity can be expressed as a function of the vegetation water content (Jackson and Schmugge, 1991).

$$\tau^c_{(f)} = b^c_{(f)} \times VWC, \tag{6}$$

where $b^c_{(f)}$ is a vegetation parameter that is dependent on vegetation type, polarization, frequency and incidence angle.

A schematic representation of the major steps involved in the soil moisture retrieval process is shown in Fig. 1. Additional information on the algorithm-specific correction models is given in Fig. 2 and Tables 3–5, and further described in the following sections.

3. Algorithms

This section introduces the theoretical basis of the algorithms, highlighting their key components and describing their general processing flow, which is schematically illustrated in Fig. 2. As mentioned earlier, in addition to the different approaches taken by each algorithm in implementing the RTE model, there will be differences associated with the choice of ancillary data, screening for unreliable data (i.e. RFI) or specific ground conditions for which reliable retrievals are not possible (i.e. frozen soils, dense vegetation, etc.), and the methods for gridding.

Information on algorithm-specific ancillary data sets and fixed parameters is provided in Table 3. We recognize that a thorough intercomparison of the algorithms would include normalization of ancillary data, flags, and gridding/posting variations. However, this could only be achieved by substantially re-coding each algorithm and is beyond the scope of this investigation.

The subset of algorithms included in this investigation was based on those that met the following requirements: (1) supports a routine product by an agency, (2) code implemented using AMSR-E Level 2A data as provided by the NSIDC, and (3) code well documented in the literature and available to us. Two algorithms used to produce routine global soil moisture products were not included since they did not meet these requirements, namely the WindSat algorithm (Li et al., 2010) and the JAXA standard algorithm (Imaoka et al., 2010; Oki et al., 2010). Li et al. (2010) have implemented a variation of the iterative optimization scheme proposed by Njoku and Li (1999); however, the parameterization

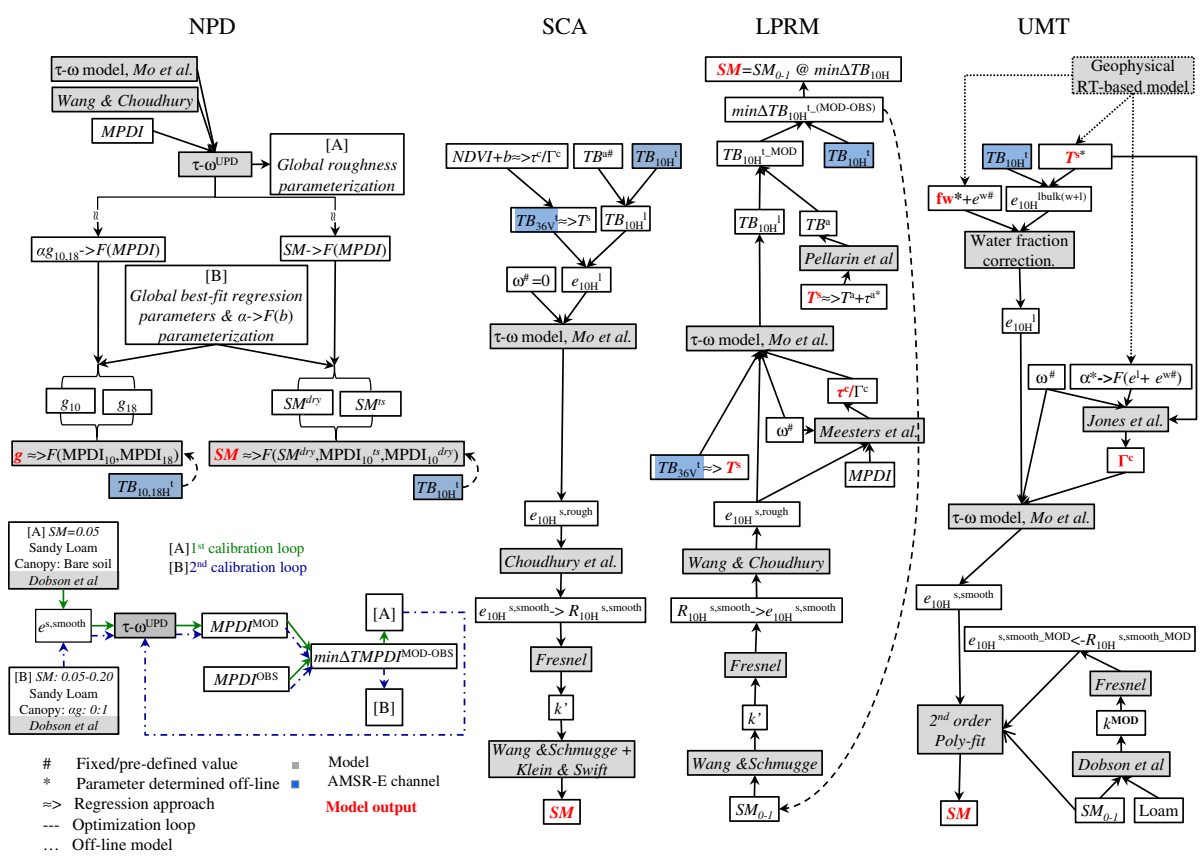

Fig. 2. Flowcharts illustrating the theoretical basis of the NPD SCA, LPRM, and UMT retrieval approach. All four approaches are based on the τ–ω model. The present operational NPD algorithm is based on a forward-based solution of the τ–ω model. The vegetation–roughness parameter *g* and *SM* are expressed as a function of $MPDI_{(f)}$. SCA is an inverse-based, single parameter retrieval model, where vegetation parameterization is done using ancillary information. LRPM retrieval is based on optimizing the difference between modeled and observed *H*-pol $T^t_{B(f,p)}$, where the modeled value is computed using forward-based solution of the RTE model. UMT partitions the composite land surface emissivity between land only and water contribution through an extra water fraction correction, where the water fraction value is determined using higher frequencies AMSR-E data. The UMT soil moisture product is derived using a theoretical $e_{(f,p)} - SM$ curve. Notes: The NPD algorithm is summarized using two flowcharts: top flowchart provides a general illustration of the overall retrieval process, while the bottom flowchart illustrates the τ–ω calibration runs. The calibration portion of the model includes two related loops, [A] (i.e. roughness calibration) and [B] (vegetation related parameterization). See Section 3.1 for more details.

Table 3
Algorithms input data and outputs.

Algorithm		Inputs		Outputs
(1) NPD	[1]	$6_{H/V}$, $10_{H/V}$, $18_{H/V}$, 89_H		SM
	[2]	Surface characteristics	FNOC	Vegetation characteristics
		Min. monthly MPDI climatology	AMSR-E	
	[3]	Regression coefficients		
(2) SCA	[1]	10.6_H, $18_{H/V}$, 23_V, 36_V, 89_V		SM
	[2]	FAO soil data base	Shape map	
		NDVI climatology	AVHRR	
		Land cover map	Landsat/UMD	
	[3]	b, h, ω, κ^{rock}, κ^{ice}		
		θ, f		
(3) LPRM	[1]	$6_{H/V}$, $10.6_{H/V}$, 36_V		SM
	[2]	FAO soil data base	GLDAS	Vegetation characteristics
	[3]	Q, h, ω, τ^a, T^{sky}, κ^{rock}, κ^{ice}, κ^{air}, θ, f		Effective (*soil*) temperature
(4) UMT	[1]	$6_{H/V}$, $10.6_{H/V}$, $18_{H/V}$, $23_{H/V}$, $36_{H/V}$, $89_{H/V}$		SM
	[2]	–		Vegetation characteristics
	[3]	ω, α, e^w, $e^{baresoil}$		Effective (*air*) temperature
		θ, f		Water fraction
		Regression coefficients		Integrated water vapor content
		Sand, clay, silt, β_d for loam		
(5) HA-ANN	[1]	$6_{H/V}$, $10_{H/V}$, $18_{H/V}$, $36_{H/V}$		SM
				Vegetation biomass

Notes: [1], [2], [3] — AMSR-E channels used in the retrieval, static global data sets, fixed parameters; not listed in the table: all approaches use the default AMSR-E land/ocean mask.

is specific to the WindSat channels and overpass times and is not easily transferable for use with AMSR-E data. Furthermore, the code was not available. JAXA products are available, but are derived from a different T_B product. In addition, the code was not available, which prevented us from implementing the JAXA algorithm with the NASA T_B input data.

3.1. Normalized Polarization Difference (NPD) algorithm

Since the NPD algorithm is the primary focus of this investigation it will be discussed in more detail than the other approaches. The algorithm is based on the radiative transfer models described above (Eqs. 3, 4a, 4b, and 6) and the assumption that atmospheric effects can be neglected without impacting soil moisture retrieval error when using the X-band frequency. Initial implementation of the original Njoku and Li (1999) approach was done using C-band observations. However, due to RFI contamination of the AMSR-E C-band data discovered after launch, especially over the U.S., the operational *SM* product is currently derived using X-band brightness temperature data which has much less RFI contamination.

The foundation of the algorithm is the use of the Normalized Polarization Difference. In should be noted that NPD and the Microwave Polarization Difference Index (MPDI) are equivalent and as shown below are computed using the same equation (equation 7); however, the developers of the alternative approaches (i.e. NPD, LPRM, HA-ANN) refer to this index in a different way.

$$MPDI_{(f)} = NPD_{(f)} = \left[T^t_{B(f,V)} - T^t_{B(f,H)}\right] / \left[T^t_{B(f,V)} + T^t_{B(f,H)}\right]. \tag{7}$$

The $MPDI_{(f)}$ is used since it can be approximated in a form that is independent of surface temperature and has separable soil moisture and vegetation dependencies. Using Eq. (5) (i.e., assuming $T^s \cong T^c$ and $\omega_{(f)} = 0$) and substituting Eqs. (4a) and (4b) (with $G(\theta) \cong 1$) and

Table 4
General RTE modeling and assumptions.

Algorithm		Some assumptions	Eq. (2) Modified equation	Eq. (3) Modified equation	Derivation of the component specific solutions
(1) NPD		$\omega = 0$ $T^c = T^s$ ω & τ^c un-polarized $T^t_B = T^l_B$ (i.e. no atm. contribution)	$T^t_B = T^l_B$	$T^l_B = T^s[1 - (1 - e^{s,rough})\Gamma^2]$	T^s — independent τ^c — *MPDI* + Eq. (3.1)
(2) SCA		$\omega = 0$ $T^c = T^s$ Constant atm. contribution	$T^t_B = const. + T^l_B$	$T^l_B = T^s[1 - (1 - e^{s,rough})\Gamma^2]$	T^s — regression τ^c — ancillary
(3) LPRM		$T^c = T^s$ ω & τ^c un-polarized	Fully solved	Fully solved	T^s — regression τ^c — *MPDI* + Eq. (3)
(4) UMT	Geophysical[a]	Ignores the surface reflection term $T^c = T^s$ ω & τ^c un-polarized	$T^t_B = T^s[\Gamma^a e^{composite} + (1 - \Gamma^a)]$	$e^{composite} = wf \times e^w + (1 - wf)e^l$ $e^l = e^s\Gamma^c + (1 - \omega)(1 - \Gamma^c)$	T^s — Eq. (2.4) Γ^a — Eq. (2.4) V — $MAWVI_{18+23}$ wf — PR_{18} + Eq. (2.4) + Eq. (3.4) Γ^c — $FI_{H,18/23}$ + Eq. (2.4) + Eq. (3.4)
	SM	$T^c = T^s$ ω & τ^c un-polarized	$T^t_B = T^l_B$	Fully solved	τ^c — α + Eq. (3)

Eq. (2): $T^t_{B(f,p)} = T^{a\uparrow}_{B(f,p)} + e^{-\tau^a_{(f,p)}}\left(1 - e^{rough}_{(f,p)}\right)\left(T^{a\uparrow}_{B(f,p)} + {}^{-\tau^a_{(f,p)}} T^{sky}_B\right)e^{-2\tau^c_{(f,p)}} + e^{-\tau^a_{(f,p)}} T^l_{B(f,p)}$

Eq. (3): $T^l_{B(f,p)} = T^s e^{rough}_{(f,p)} e^{-\tau^c_{(f,p)}} + T^c\left(1 - \omega_{(f,p)}\right)\left(1 - e^{-\tau^c_{(f,p)}}\right) + e^{-\tau^c_{(f,p)}} T^c\left(1 - \omega_{(f,p)}\right)\left(1 - e^{-\tau^c_{(f,p)}}\right)\left(1 - e^{rough}_{(f,p)}\right)$

Notes: Equation numeration in the table: the 1st number refers to the complete RTE (2) or the τ–ω model (3), respectively; the 2nd number, if present, corresponds to the algorithm ID number listed in the first column of this table. For example, Eq. (3.1) indicates NPD specific solution of the τ–ω model.

[a] The UMT geophysical retrieval model provides information about the additional land surface parameters (i.e. effective temperature, fraction of open water, etc.) required by the soil moisture retrieval algorithm (see Section 3.4).

Table 5
Geophysical retrieval models.

Algorithm	(1) Vegetation and roughness	(2) Temperature	(3) Atm. effects	(4) Additional	Dielectric mixing
(1) NPD	Njoku and Chan (2006) *MPDI-based* Wang and Choudhury (1995) $h-Q$ Specific values: $\omega=0$, $\tau^c F(MPDI^{dry})$, $hG=-$, $Q=0.184$	–	–		Dobson et al. (1985) *Fixed soil properties*
(2) SCA	Jackson and Schmugge (1991) *NDVI climatology* Choudhury et al. (1979) h Specific values: $\omega=0$, $\tau^c F(NDVI)$, $hG=0.1\times\cos^2\theta$, $Q=-$	De Jeu and Owe (2003) *Regression*, 37(V)	– *Constant value*		Wang and Schmugge (1980) Klein and Swift (1977) *Spatially variable soil properties*
(3) LPRM	Meesters et al. (2005) *MPDI-based inversion of the RTE* Wang and Choudhury (1995) $h-Q$ Specific values: $\omega=0.06$, $\tau^c F(MPDI)$, $hG=0.18\times 1$, $Q=0.127$	De Jeu and Owe (2003) *Regression*, 37(V)	Pellarin et al. (2003) *RTE-based solution; regression model expressing the τ^a as a function of air temperature*		Wang and Schmugge (1980) *Spatially variable soil properties*
(4) UMT	Jones et al. (2011) *Slope-based inversion of the RTE* – *Through* Γ^c Specific values: $\omega=0.06$, $\tau^c F(\alpha)$, $hG=-$, $Q=-$	Jones et al. (2010) *RTE-based inversion*, 23(V)	Wentz et al. (2000) *Regression model expressing the τ^a s a function of oxygen and water vapor*	Jones et al. (2010) *Water fraction correction*	Dobson et al. (1985) *Fixed soil properties*

Eq. (7), we obtain:

$$T^l_{B(f,p)} = T^s\left\{1-\left[\left(1-Q_{(f)}\right)R^{s,smooth}_{(f,p)} + Q_{(f)}R^{s,smooth}_{(f,q)}\right]e^{\left[-\alpha_{(f)}g\right]}\right\}, \tag{8}$$

where

$$\alpha_{(f)}g = h_{(f)} + \left(2b^c_{(f)}\times VWC\right)/\cos\theta. \tag{9}$$

As defined earlier $Q_{(f)}$ and $h_{(f)}$ are roughness parameters.

A key concept introduced here is the parameter g, which is a vegetation/roughness surface characteristic representing combined *RMS* height and *VWC* information. $\alpha_{(f)}$ is a frequency-dependent coefficient. The applicability of this lumped parameter representation is discussed in Njoku and Chan (2006).

Combining Eqs. (7) and (8), and assuming that the atmospheric effects are negligible (so that we can use $T_{B(f,\,p)}{}^t = T_{B(f,\,p)}{}^l$), yields:

$$MPDI_{(f)} = A_{(f,SM)}\left(1-2Q_{(f)}\right)/\left\{1+B_{(f,SM)}\left(e^{\left[\alpha_{(f)}g\right]}-1\right)\right\}, \tag{10}$$

where

$$A_{(f,SM)} = \left[e^{smooth}_{(f,V)} - e^{smooth}_{(f,H)}\right]/\left[e^{smooth}_{(f,V)} + e^{smooth}_{(f,H)}\right] \tag{11a}$$

$$B_{(f,SM)} = 2/\left[e^{smooth}_{(f,V)} + e^{smooth}_{(f,H)}\right]. \tag{11b}$$

$A_{(f,SM)}$ and $B_{(f,SM)}$ are both functions of *SM*, and $A_{(f,SM)}$ represents the $MPDI_{(f)}$ of bare, smooth soil.

It was shown in Njoku and Chan (2006) that Eq. (10) can be further approximated as:

$$MPDI_{(f)} \approx A_{(f,SM)}\left(1-2Q_{(f)}\right)e^{-\beta_{(f)}\alpha_{(f)}g}, \tag{12}$$

where $\beta_{(f)}$ is a coefficient that is approximately independent of soil moisture. Values for the coefficients $Q_{(f)}$, $\beta_{(f)}$ and $\alpha_{(f)}$ were obtained for AMSR-E as described below.

The parameters $h_{(f)}$ and $Q_{(f)}$ have similar impact on $MPDI_{(f)}$ (see Fig. 1 in Njoku and Chan, 2006) and consequently there is some redundancy in varying both of these parameters to establish best fits. Therefore, $h_{(f)}$ (incorporated in the $\alpha_{(f)}g$ term) was selected to represent the spatial variability, while $Q_{(f)}$ was treated as a fixed global factor. $Q_{(f)}$ was determined for each frequency by calibrating Eq. (12) to the AMSR-E computed $MPDI_{(f)}$ values over two desert regions with smooth topography (Niger and Saudi Arabia, see Njoku and Chan (2006) for the specific coordinates of each box; $Q^{NPD,Niger}_{10.7} = 0.198$ and $Q^{NPDS.Arabia}_{10.7} = 0.184$). The radiative transfer runs were carried out assuming bare, smooth, dry land surface conditions with $h_{(f)} = 0$ and $SM = 0.05\ m^3/m^3$. As computed, the $Q_{(f)}$ values estimated over these calibration sites would represent minimum roughness conditions. The lower Saudi Arabia $Q_{(f)}$ value was selected as a global parameter. Spatial variations in surface roughness were then accounted for by allowing $h_{(f)}$ to vary globally.

The coefficients $\alpha_{(f)}$ and $\beta_{(f)}$ were determined using a similar approach. Simulations performed to estimate these parameters were done using the Dobson dielectric model (Dobson et al., 1985) for dry ($SM = 0.05\ m^3/m^3$) to moderate ($SM = 0.20\ m^3/m^3$) soil moisture conditions assuming uniform (sandy loam) soils.

Calibration of $\alpha_{(f)}$ was performed over a region of naturally varying vegetation and roughness that had uniform dry soil moisture (portions of Chad, Sudan, and the Central African Republic). AMSR-E observations for a dry month (March 2004) over this domain were used to estimate $\alpha_{(f)}$.

The NPD AMSR-E soil moisture retrieval algorithm is derived from Eq. (12). Njoku and Chan (2006) examined the sensitivity of the function $A_{(f,SM)}(1-2Q_{(f)})$, which characterizes the soil moisture response. The function shows good sensitivity over the full soil moisture range, although the sensitivity decreases at higher moisture values (see Fig. 4 of Njoku and Chan, 2006).

To implement the retrieval, Eq. (12) can be inverted and written in the form:

$$A_{(SM)} = \frac{1}{(1-2Q)}(MPDI)e^{\beta\alpha g}, \tag{13}$$

where the subscript f has been dropped since the retrieval algorithm uses only the 10.7 GHz frequency, and $A_{(SM)}$ was defined in Eq. (11a). Once $A_{(SM)}$ is determined using the observed *MPDI* and the roughness/vegetation correction factor ($\beta\alpha g$), Eq. (13) can be used with the Fresnel equations, a global soil texture database, and a dielectric model to determine soil moisture. Alternatively, a linear approximation to the relationship between $A_{(SM)}$ and soil moisture can be used and Eq. (13) written as:

$$SM = a_0 + a_1(MPDI)e^{\beta\alpha g}, \tag{14}$$

where a_0 and a_1 are coefficients that are determined empirically. Eq. (14) can also be expressed in time-differenced relative change form, where soil moisture is expressed as a departure from a minimum or "dry" condition at each location (grid point or pixel). Using this formulation the coefficient a_0 drops out:

$$SM = SM^{dry} + a_1\left(MPDI - MPDI^{dry}\right)e^{\beta\alpha g}. \tag{15}$$

Similarly, we can write the exponential factor as:

$$\beta\alpha g = b_1 + b_2 \ln\left[MPDI^{dry}\right]. \tag{16}$$

The optimum time window for computing $MPDI^{dry}$ for use in these equations depends on the specific location.

3.2. SCA

The Single Channel Algorithm utilizes the single frequency/polarization instrument channel that is most sensitive to soil moisture, and relies on ancillary data to perform corrections for other factors (including *VMC*) that affect the retrieval. As with the NPD algorithm, the AMSR-E implementation of SCA assumes that $\omega = 0$ and that the atmospheric contribution is minimal. As a result Eqs. (4a), (4b) and (5) can be used:

$$T^{l}_{B(f,p)} = T^{s}\left\{1 - \left(1 - e^{s,rough}_{(f,p)}\right)\left(e^{\left[-\tau^{c}_{(f,p)}/\cos\theta\right]}\right)^{2}\right\}. \tag{17}$$

Combining Eqs. (4a), (4b) and (17) with $Q_{(f)} = 0$ and $G(\theta) = \cos^2\theta$ following the model of Choudhury et al. (1979), and inverting the resulting equation, allows us to compute the smooth surface reflectivity:

$$R^{s,smooth}_{(f,p)} = \left\{1 - \frac{T^{l}_{B(f,p)}}{T^{s}}\right\}e^{\left[h_{(f)}\cos^2\theta + 2b^{c}\times VWC/\cos\theta\right]}. \tag{18}$$

For AMSR-E implementation, the physical temperature of the soil is approximated using the vertically polarized Ka-band AMSR-E brightness temperature (De Jeu and Owe, 2003). The roughness parameter $h_{(f)}$ is assumed constant at the global scale and is assigned the value $h = 0.1$.

Jackson et al. (1999) showed that *VWC* can be linearly related to *NDVI*. In the current investigation *VWC* is estimated using *NDVI* monthly climatology derived using AVHRR observations from the 1981–1999 time period.

The smooth surface reflectivity (Eq. 18) is related to the dielectric properties of the soil through the Fresnel reflectivity model. Eq. (1a) can be inverted to estimate the dielectric constant (Eq. 19).

$$\kappa_{(f,H)} = \sin^2\theta + \cos^2\theta \times \left[\frac{\sqrt{R^{s,smooth}_{(f,p)}} + 1}{\sqrt{R^{s,smooth}_{(f,p)}} - 1}\right]^2. \tag{19}$$

The Wang and Schmugge (1980) dielectric model is then used to relate the real part of the dielectric constant to the soil moisture using ancillary data describing the soil texture. The soil texture data are obtained from the global soil properties data base described in Reynolds et al. (2000) (http://www.ngdc.noaa.gov/ecosys/cdroms/reynolds/reynolds/reynolds.htm).

The SCA has been implemented using the NASA-based L2A brightness temperature data. Currently the retrieval is carried out utilizing the horizontally polarized X-band AMSR-E observations (and using the fixed value of θ for AMSR-E). It has also been applied to the JAXA brightness temperature data. The final soil moisture estimates are outputted into the original resolution of the T_B (orbital footprint resolution).

3.3. LPRM

LPRM is a multi-parameter retrieval model that provides estimates of soil moisture, optical depth and effective temperature without requiring the use of dynamic ancillary data. A schematic representation of the model is given in Fig. 2. LPRM uses Eqs. (2) and (3) to calculate $T^{t}_{B(f,p)}$ for a range of soil moisture values. Utilizing two polarizations and making the assumptions discussed below allows the simultaneous estimation of *SM* and vegetation optical depth (τ^c) by minimizing the difference between observed and modeled $T^{t}_{B(f,h)}$. LPRM has been applied using data from different frequencies and satellites (Owe et al., 2008). For consistency with the other algorithms described in this paper, only the X-band parameterization is presented here.

The smooth soil reflectivity is computed based on the Wang and Schmugge dielectric mixing model and the Fresnel reflectivity equations for each soil moisture estimate in the optimization process. With regard to parameters, as with SCA, those related to roughness ($h_{(10.7)} = 0.18$; $Q_{(10.7)} = 0.127$) and the single scattering albedo ($\omega_{(10.7,H=V)} = 0.06$) are spatially and temporally fixed. As in the other algorithms presented here, it is assumed that T^s and T^c are approximately equal. The effective soil temperature is calculated outside the optimization loop using 36.5 GHz, *V*-polarized AMSR-E data as described in Holmes et al. (2009). As with the NPD algorithm, vegetation parameterization ($\tau^{c}_{(f,p)}$) is based on a function of $MPDI_{(f)}$, however, as discussed below, LPRM adopts somewhat different approach.

The optical depth is determined using the analytical solution to the radiative transfer equation as described by Meesters et al. (2005). An important assumption of LPRM is that the single scattering albedo and optical depth are polarization independent at the satellite spatial scale ($\omega_{(f,H=V)} \rightarrow \omega_{(f)}$ and $\tau^{c}_{(f,H=V)} \rightarrow \tau^{c}_{(f)}$). Polarization independence of the vegetation optical depth at satellite scale was tested and confirmed by Owe et al. (2001). It can be shown by substituting Eq. (3) into Eq. (7) that the $\tau^{c}_{(f)}$ can be calculated through the following system of equations:

$$\tau^{c}_{(f)} = \cos\theta \ln\left[ad + \sqrt{(ad)^2 + a + 1}\right], \tag{20}$$

where

$$a = \frac{1}{2}\left[\frac{e^{s,rough}_{(f,V)} - e^{s,rough}_{(f,H)}}{MPDI_{(f)}} - e^{s,rough}_{(f,V)} - e^{s,rough}_{(f,H)}\right]$$

$$d = \frac{\omega_{(f)}}{2\left(1 - \omega_{(f)}\right)}.$$

The LPRM operates by first computing $\tau^{c}_{(f)}$ for a given soil moisture using Eq. (20) (atmospheric effects not included in this step). Then, this value of $\tau^{c}_{(f)}$ is used in Eq. (3) to compute $T^{l}_{B(f,p)}$ as discussed above.

The atmospheric contribution required for Eq. (2) in order to estimate $T^{t}_{B(f,p)}$ is determined using the model of Pellarin et al. (2003):

$$T^{a(\uparrow\approx\downarrow)}_{B(f,p)} = T^{a}\left(1 - e^{\left[-\tau^{a}_{(f,p)}/\cos\theta\right]}\right) \quad 21$$

$$T^{sky\downarrow}_{B(f,p)} = T^{sky}e^{\left[-\tau^{a}_{(f,p)}/\cos\theta\right]}, \text{ where } T^{sky} = 2.7 \text{ K}. \tag{22}$$

This approach assumes that the up- and down-welling atmospheric contributions are approximately equal and introduces two new unknowns: equivalent atmospheric temperature (T^a) and atmospheric optical thickness ($\tau^{a}_{(f,p)}$), both of which are functions of altitude and air temperature. In the LPRM, T^a is expressed through a regression relationship as a function of T^s, while $\tau^{a}_{(f,p)}$ is assigned a globally and temporally fixed best estimate value of 0.011 determined from the literature (Colwell et al.,1983). This two-step cycle is repeated varying the soil

moisture to find the value of soil moisture that minimizes the difference between the computed and observed $T^t_{B(f,p)}$.

The publicly distributed LPRM product is a composite C-/X-band product designed to optimize soil moisture retrieval over RFI affected areas (http://gcmd.nasa.gov/records/GCMD_GES_DISC_LPRM_AMSRE_SOILM2_V001.html). The approach performs the retrievals separately for the C- and X-channels by using the L2A NASA brightness temperature data and varying the frequency dependent parameters (i.e. roughness parameters, single scattering albedo) according to the channel that is used. Retrievals are stored separately at the orbital footprint resolution. Whether or not the C- or X-band retrieval is used in the publically distributed gridded global product is determined based on the presence of RFI contamination.

3.4. UMT

UMT is also a multi-parameter retrieval model that combines two sub-algorithms: (Algorithm 1) a geophysical retrieval model that derives effective surface air temperature ($T^{effective}$), fraction of open water (wf), total vertical water vapor content of the atmosphere (V), and vegetation transmissivity ($\Gamma^c_{(f)}$) and (Algorithm 2) a soil moisture retrieval model. The UMT flowchart shown in Fig. 2 summarizes only the soil moisture component (Algorithm 2). Note that (Algorithm 1) the geophysical retrieval model uses a simplified RTE solution derived by ignoring the surface reflection terms in both Eqs. (2) and (3) and utilizes an iterative optimization procedure, while (Algorithm 2) the soil moisture algorithm uses the full quadratic τ–ω model (Eq. 3). As with the NPD and the LPRM algorithms, UMT assumes that the single scattering albedo, optical depth and atmospheric transmissivity are not polarization dependent.

UMT models the composite land surface emissivity ($e^{composite}_{(f,p)}$) as a weighted combination of the open water and land only contribution according to

$$e^{composite}_{(f,p)} = wf \times e^{w}_{(f,p)} + (1-wf) \times e^{l}_{(f,p)}. \tag{23}$$

The resulting simplified versions of Eqs. (2) and (3) generated by ignoring the surface reflection term ($1 - e^{rough}_{(f,p)}$) that are used by (Algorithm 1) the geophysical retrieval model are given in Eqs. (24) and (25), respectively.

$$e^{l}_{(f,p)} = e^{s}_{(f,p)}\Gamma^c_{(f)} + \left(1-\omega_{(f)}\right)\left(1-\Gamma^c_{(f)}\right) \tag{24}$$

and

$$T^{l}_{B(f,p)} = T^s\left[\Gamma^a_{(f)}e^{composite}_{(f,p)} + \left(1-\Gamma^a_{(f)}\right)\frac{T^a}{T^s}\right]. \tag{25}$$

The geophysical parameters necessary to solve Eqs. (23)–(25) are estimated using multiple frequencies (H- and V-polarized 18.7 GHz and 23.8 GHz brightness temperature data) and several microwave indices, including the Microwave Atmospheric Water Vapor Index ($MAWVI_{(f)}$), the Frequency index ($FI_{(f,\,h)}$), and the Polarization Ratio ($PR_{(f)}$) defined as follows:

$$MAWVI_{(18H,V;23H,V)} = \left[T^t_{B(23,V)} - T^t_{B(23,H)}\right] / \left[T^t_{B(18,V)} - T^t_{B(18,H)}\right] \tag{26a}$$

$$FI_{(18H;23H)} = \left[T^t_{B(23,H)}\right] / \left[T^t_{B(18,H)}\right] \tag{26b}$$

$$PR_{(18H,V)} = \left[T^t_{B(18,H)}\right] / \left[T^t_{B(18,V)}\right] \tag{26c}$$

V is determined using the $MAWVI_{(f)}$ index and some additional predefined frequency specific parameters describing the oxygen and water vapor absorption properties [see Table II of Jones et al. (2010)]. $\Gamma^a_{(f)}$ used in the computation of the effective temperature (Eq. 25) can be expressed as a function of the integrated atmospheric water vapor. The simplified RTE model given in Eqs. (23)–(25) is substituted into the $PR_{(f)}$ and the $FI_{(f,\,h)}$ expressions and then inverted to estimate wf and $\Gamma^c_{(f)}$, respectively. It is assumed that the cloud liquid water effects at these higher frequencies are minimal and that the single scattering albedo and transmissivity are polarization independent. The exact formulations for wf, V and $\Gamma^c_{(f)}$ can be found in Jones et al. (2010) and are not included in this paper. It should also be noted that the effective temperature is estimated as part of the RTE-based solution.

The $\Gamma^c_{(f)}$ derived from the geophysical retrieval model and the $\tau^c_{(f)}$ used in the soil moisture algorithm differ: as noted earlier, the soil moisture retrieval algorithm (i.e. Algorithm 2) uses the complete $\tau - \omega$ model, while (Algorithm 1) uses a simplified version developed under the assumption of no surface reflection. Thus, the $\tau^c_{(f)}$ used for the computation of the SM values is estimated by inverting the land–water emissivity slope index ($\alpha_{(f)}$), given in Eq. (27), in terms of the τ–ω model (Eq. 3).

$$\alpha_{(f)} = \left(e^{composite}_{(f,V)} - e^{w}_{(f,V)}\right) / \left(e^{composite}_{(f,H)} - e^{w}_{(f,H)}\right), \tag{27}$$

where $e^{w}_{(f,p)}$ is considered constant and the effective composite emissivity is estimated using Eq. (23) (the atmospheric effect is accounted for through the $\Gamma^{\alpha}_{(f)}$ term). The resulting formulation for $\tau^c_{(f)}$ is given in Eq. (28).

$$\tau^c_{(f)} = -\log\left[\frac{-B-\sqrt{B^2-4AC}}{2A}\right], \tag{28}$$

where

$$A = \left(1-\omega_{(f)}\right)\left(R^{s\#}_{(f,V)} - \alpha_{(f)}R^{s\#}_{(f,H)}\right)$$

$$B = \alpha_{(f)}e^{s\#}_{(f,H)} - e^{s\#}_{(f,V)} + \left(1-\omega_{(f)}\right)\left(\alpha_{(f)}R^{s\#}_{(f,H)} - R^{s\#}_{(f,V)} + 1-\alpha_{(f)}\right)$$

$$C = \left(1-\omega_{(f)}\right)\left(\alpha_{(f)}-1\right) + e^{w\#}_{(f,V)} - \alpha_{(f)}e^{w\#}_{(f,H)},$$

where # indicates predefined values for dry bare soil emissivity ($e^{s\#}_{(f,p)}$, where $R^{s\#}_{(f,p)} = 1 - R^{s\#}_{(f,p)}$) and open water emissivity ($e^{w\#}_{(f,p)}$). $\omega_{(f)}$ is fixed to 0.06; see Table II of Jones et al. (2010).

As described previously for the NPD algorithm increasing roughness and vegetation can have similar effects on the observed microwave emission. Since $\alpha_{(f)}$ was estimated using the observed $T^t_{B(f,p)}$, the resulting $\tau^c_{(f)}$ incorporates roughness effects. This is also true for the LPRM $\tau^c_{(f)}$ approach. Thus, unlike the previous approaches, where the roughness effect was estimated by using a separate roughness correction step, the UMT approach has a single correction step that incorporates both vegetation and roughness, which is accomplished through the $\alpha_{(f)}$ derived vegetation parameter.

The soil emissivity $e^{s,smooth}_{(f,p)}$ is estimated by inverting the τ–ω model as shown below.

$$e^{s,smooth}_{(f,p)} = \left[e^{l}_{(f,p)} - Ae^{\left[-\tau^c_{(f)}/\cos\theta\right]} - A\right] / \left[e^{\left[-\tau^c_{(f)}/\cos\theta\right]}(1-A)\right], \tag{29}$$

where

$$A = \left(1-\omega_{(f)}\right)\left(1-e^{\left[-\tau^c_{(f)}/\cos\theta\right]}\right)$$

and

$$e^{l}_{(f,p)} = \left(\frac{T^t_{B(f,p)}}{T^{effective}} - wf \times e^{w\#}_{(f,p)}\right) / (1-wf).$$

Finally, *SM* is estimated utilizing a theoretical $SM - e^{s,smooth}_{(f,p)}$ polynomial model based on the Dobson dielectric model for loamy soils.

The current version of the UMT code ingests the 25 km EASE grid brightness temperature data provided through NSIDC and all products generated by the algorithm are publicly available (http://nsidc.org/data/nsidc-0451.html).

3.5. HA-ANN

HA-ANN makes use of the Artificial Neural Network (ANN) training technique to perform *SM* retrieval through a statistical inversion of the τ–ω model. There are several additional features that differentiate HA-ANN from the rest of the approaches discussed in this paper: the algorithm incorporates a disaggregation step (the final soil moisture product is provided at finer resolution as compared to the standard 25 km grid), the algorithm was originally set up to ingest JAXA brightness temperature estimates, and the soil moisture estimation is based only on vertically polarized C-band data, which is different than the setup employed by the NPD algorithm. Therefore, the approach will not be included in the comparative overview presented later in this paper. We have included this algorithm to be comprehensive based upon the restrictions we mentioned earlier on algorithms; however, only a brief discussion of the major components is provided.

Essentially ANN can be regarded as a complex and sophisticated classification scheme (Atkinson and Tatnall, 1997; Mas and Flores, 2008). As with the traditional techniques (supervised, fuzzy, maximum likelihood, etc.), ANN requires a priori knowledge and reasonable physical constraints, however, because it does not rely on any assumptions it allows the use of different data types and adequately represents nonlinear relationships (Atkinson and Tatnall, 1997; Hornik et al., 1989; Lek et al., 1996; Mas and Flores, 2008). ANN can be used for inverting complex models such as RTE, without the constraints imposed by many simplified inversion algorithms, provided that the training process is performed correctly.

Prior to executing the ANN component of the algorithm, all brightness temperature data necessary for the algorithm are disaggregated to the spatial resolution of the AMSR-E Ka-band (~10 km × 10 km) using the Smoothing Filter-based Intensity Modulation (SFIM) technique described in Santi (2010). Spatial enhancement is done by utilizing a Ka-band ratio factor computed as

$$\left[T^{Org}_{B(Ka,p)}\right] / \left[T^{Up-scaled}_{B(Ka,p)}\right], \tag{30}$$

where $T^{Org}_{B(Ka,p)}$ represents the T_B value obtained at the original Ka-band resolution, while $T^{Up\text{-}scaled}_{B(p,Ka)}$ is an up-scaled T_B value representative of the lower frequency footprint.

Inputs required by the HA-ANN ANN component include ANN specific configuration files, *V*-polarized C- and Ka-band observations and two $MPDI_{(f)}$ indices developed using X- and Ku-band brightness temperature data, respectively. The ANN configuration files (one for each overpass) are generated by the training process, which is perhaps the most important step in the implementation of the algorithm. These files contain the architecture of the already trained ANNs. The training process and the definition of the ANN configuration files are carried out separately from the online process, before the application of the algorithm. However, the ANN configuration can be updated in order to improve the retrieval accuracy by repeating the training with a new dataset. The training process is based, in this case, on both simulated data (using the τ–ω model) and experimental measurements [derived from the existing JAXA $T^t_{B(f,p)}$ archive (2003–2004), which contains AMSR-E measured T_B and ground measurements of *SM* acquired over two experimental watersheds located in Mongolia and Australia]. The experimental data were also used for deriving the T_B simulations, in order to keep the consistency between simulated and observed T_B. On the other hand, RTE model simulations provide a sufficient sampling size for the training step and provided a variety of surface conditions for the training process.

As with the rest of the algorithms, HA-ANN excludes RFI contaminated pixels and does not perform retrievals over snow covered areas or under conditions of frozen soils and dense vegetation. The detection of densely vegetated areas and the evaluation of the effect of light vegetation on the *SM* retrieval are performed using *MPDI* computed using 10.7 and 18.7 GHz data. *MPDI* sensitivity to varying vegetation was tested over a site located in Africa (0°–20°N,16°–17°E).

A more detailed description of the approach and examples of the output products can be found in Santi et al. (2012).

4. Synopsis

Before inter-comparing the theoretical background of the individual algorithms' components it is helpful to demonstrate the variability in the final soil moisture products developed by these approaches Spatial maps of some basic descriptive statistics are shown in Fig. 3. These are based on 8 years of data starting with 2003. The STDEV illustrate the variability in terms of range of soil moisture. The resulting maps clearly illustrate the large differences that can occur between the alternative AMSR-E products. The algorithm specific range values, shown in the last row of Fig. 3, were computed excluding the upper and lower 2.5 percentiles, which was done to avoid outliers. Overall, all products show reasonable spatial variability, however, the patterns do not always match. This discrepancy is most evident over areas that are characterized with less "homogenous" ground conditions and more profound seasonality such as the Northern latitudes Europe. As stated previously, the goal of including this analysis is not to compare or assess the algorithm performance, but to demonstrate the difference in the soil moisture products despite the common theoretical background. These results will also aid us in the interpretation of the individual approaches and their assumptions as well as help us to identify the algorithms' components that are most likely to impact the observed difference in resulting range of soil moisture.

Section 3 described each algorithm separately and linked the individual solutions to the RTE presented in Eqs. (2) and (3). In an effort to solve these equations each algorithm goes through several major steps, including selection of modeling approach (Fig. 2). Then in order to reduce the dimensionality of unknown parameters certain assumptions are made, which leads to simplification of these main equations (Table 4). Lastly, the simplified equations are parameterized using both fixed and dynamic parameterization approaches that allow accounting for the spatial and temporal variability in certain parameters such as vegetation and effective temperature (Table 3 and 5).

4.1. Modeling approach

Fig. 2 shows how each algorithm implements a slightly different modeling approach (NPD-empirical implementation of a forward-based model, SCA-inverse, LPMR-forward, UMT-combined). A few major differences in terms of RTE mode implementation should be noted. Some of the geophysical parameters in the forward-based models such as LPRM and UMT (geophysical retrieval model) are determined simultaneously, while the inverse-based model, SCA, requires that all parameters are known a priori. If the parameters are properly accounted for and are comparable between the approaches, solving the RTE in an inverse as opposed to a forward mode should produce similar results. That is to say the modeling approach alone is not expected to generate major differences in retrievals.

4.2. Assumptions

Overall, the assumptions employed by the algorithms can be grouped in 3 major categories: canopy ($\omega_{(f,p)} = 0$, $\omega_{(f,H)} = \omega_{(f,V)}$,$\tau^c_{(f,H)} = \tau^c_{(f,H)}$), temperature ($T^c \cong T^s$) and atmosphere ($T^t_{B(f,p)} = T^l_{B(f,p)}$) related

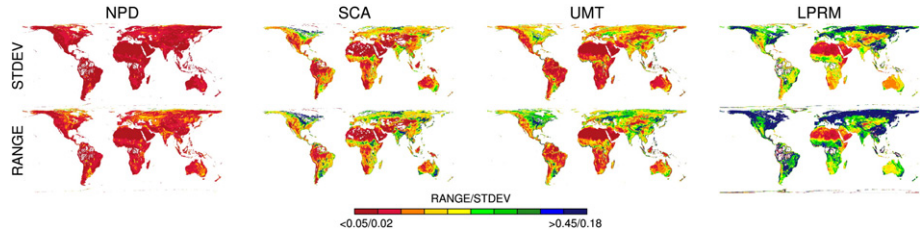

Fig. 3. Basic descriptive statistics of the four soil moisture products discussed in the paper. Statistics were calculated for the 2003–2010 time period. The RANGE was computed by excluding the upper and lower 2.5 percentiles to avoid outliers. Dark red color indicates areas, where the RANGE values are below 0.05 m^3/m^3, and the STDEV values are below 0.02 m^3/m^3, while the dark blue is associated with areas, where the RANGE values are above 0.45 m^3/m^3, and the STDEV values are above 0.18 m^3/m^3. The range of soil moisture captured by each product is associated with the temporal variability of each product.

(Table 4). The UMT and NPD algorithms introduce a few additional and not so common assumptions such as minimal impact of the surface reflectance term in Eq. (2) and separable *SM* and vegetation dependences in the *MPDI*, respectively. The direct effect of these assumptions in terms of solving Eqs. (2) and (3) is shown in Table 4. Nevertheless, in terms of retrieval accuracy, as discussed in Sections 2 and 3, the overall impact of these assumptions on the final estimates is considered negligible at the AMSR-E satellite footprint spatial scale and at the microwave frequency range used for soil moisture monitoring (i.e. $f \leq 11$ GHz). Thus, it follows that the differences observed in the final retrievals would be caused by the geophysical parameterization.

4.3. Parameterization

The key differences between the algorithms related to the parameterization modules are summarized in Table 5. Each component included in this table will be discussed separately.

4.4. Atmospheric effects

The most noticeable difference in Table 4, which shows the algorithm specific RTE, is related to Eq. (2) and the way how each approach accounts for the atmospheric effects. As we can see from column 3 of Table 5 the atmospheric contribution is modeled in one of three ways: (1) assume no atmospheric contribution; (2) assume a constant value; or (3) use a radiative transfer-based solution (Pellarin et al., 2003). The UMT approach offers a variation of these by expressing $\tau^a_{(f)}$ as a function of the total vertical water vapor content of the atmosphere (V) (Jones et al., 2010). However, the UMT atmospheric parameterization approach is implemented only in the geophysical retrieval model, which provides the effective temperature and water fraction estimates ingested by the soil moisture algorithm. In the UMT soil moisture retrieval model the X-band acquired data are corrected only for the impact of oxygen absorption. This correction is spatially and temporally invariable and has minimal impact on the observed radiation at C- and X-frequencies.

When treated as a constant (i.e. SCA), the typical value assumed for the combined atmospheric and sky radiation is ~3 K. The main difference between (1)–(2) and (3) is that the RTE modeling allows to account for the spatial and temporal variability in the atmospheric contribution. To explore how different the estimated atmospheric contribution is as compared to assuming 0 K and ~3 K we applied the model of Pellarin et al. (2003) using the LPRM model. Several different scenarios were run in order to explore the sensitivity of the atmospheric T_B to the ground surface conditions by varying the soil texture, T^s, and *SM*. Each scenario was run for the full transmissivity range of 0 to 1 (plotted on the x-axis). Results are shown in Fig. 4.

A few features of Fig. 4 stand out. First, T^s and soil texture have relatively small impacts on the estimated atmospheric T_B as compared to the variability in soil moisture and vegetation conditions. At first glance it appears that adopting a fixed value would result in over- or under-correction depending on canopy density and soil wetness. Making the assumption that no atmospheric correction is required may lead to overestimation of T^l. However, some additional details need to be considered, such as the fact that over densely vegetated areas soil moisture retrieval is not attempted (i.e. $0 < \Gamma^c_{(f)} < 0.25$ at $\theta = 55°$ and $\tau^c_{(f)} = 0.8$, where $\Gamma^c_{(f)} = \exp(-\tau^c_{(f)}/\cos\theta)$; 0.8 is LPRM dense vegetation threshold), which will reduce the adjustment range. For average soil moisture conditions (i.e. 0.1 to 0.3 m^3/m^3) $T^t_B - T^l_B$ ranges between ~0.5 K over densely vegetated areas (at $\tau^c_{(f)} = 0.8$) and ~4 K over bare surface conditions (computed as an average value of the 0.1, 0.2 and 0.3 soil moisture curves), which is not very different compared to making no correction or using a 3 K fixed value.

A more important question is what would be the impact of this change on the estimated soil moisture retrieval. Soil moisture sensitivity (S^{SM}) to change in T_B, where $S^{SM} = \Delta T_B/\Delta SM$, is dependent on numerous parameters, including moisture content, roughness, and vegetation density as well as other factors. Based on published data, S^{SM} can vary from 2 K to 5 K per 0.01 m^3/m^3 at L-band (Schmugge, 1980; Ulaby et al., 1986); S^{SM} is expected to be slightly lower at X-band as T_B sensitivity to *SM* generally decreases with an increase in frequency, see Schmugge (1980).

Consequently, this analysis shows that the assumption of no or minimal atmospheric contribution is a reasonable simplification at $f \leq 11$GHz. However, this may not be a valid assumption when using higher frequencies for the estimation of the ancillary land surface parameters. Our analyses indicated that the atmospheric correction cannot explain the reduced sensitivity of the NPD algorithm or the observed differences between the retrievals, and it is not likely that it will help improve the range of the retrieved *SM* values.

4.5. Effective temperature

The soil moisture algorithms selected here estimate the effective temperature in one of two general ways (1) using linear regression-based techniques or (2) by inverting the RTE model using higher frequency AMSR-E channels. In the first T^s approach, used by SCA and LPRM, regression coefficients are derived using a limited station data base, which may contribute to spatial representativeness associated errors. Furthermore, the regression based T^s estimation is typically done using *V*-pol. 36.5 GHz brightness temperature observations, while the RTE-based UMT approach uses *V*-pol. 23.8 GHz brightness temperature observations. Both T^s approaches should provide comparable estimates of T^s in terms of magnitude and range. However, as the 23.8 GHz frequency is closest to the lowest water vapor absorption line (22.235 GHz), it is likely that the T^s contribution is smaller in the 23.8 GHz channel as it is sensing the lower atmosphere. Therefore, it is expected that the atmospheric effects will be lower at 36.5 GHz (Njoku et al., 2004; Qiu et al., 2007; Ulaby et al., 1981). Furthermore, in addition to the frequency difference, the site specific nature of the regression approach as well as the extra water fraction correction employed in the RTE approach are likely to produce differences in the T^s estimates ingested by the individual *SM* algorithms. It is also reasonable to expect that the effective temperature inputs used by SCA and

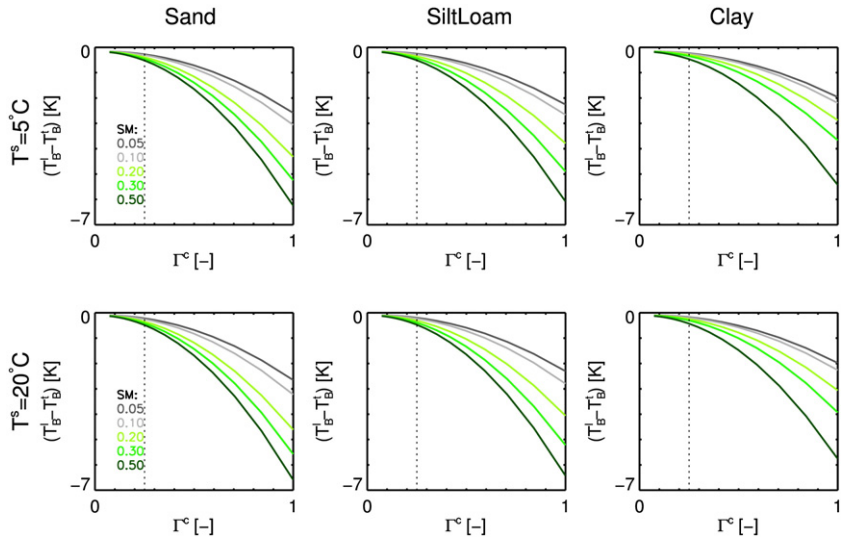

Fig. 4. Simulated total atmospheric contribution computed using the LPRM set up, where the up-/down-welling and cosmic radiation components are estimated following Pellarin et al. (2003). Simulations were carried out by fixing the soil properties, soil effective temperature and soil moisture.

LPRM are very similar since they both employ similar *SM* regression-based models to estimate the effective temperature. However, as seen in Fig. 3 SCA and UMT produce similar soil moisture results, while SCA and LPRM differ significantly in terms of the range of soil moisture. Uncertainties in T^s can contribute to errors in the final soil moisture retrievals (Holmes et al., 2012; Parinussa et al., 2011); however, assuming that the effect of open water bodies or standing water is properly accounted for, it is not likely that T^s can explain the differences in the range of soil moisture produced by the algorithms.

4.6. Vegetation parameterization & roughness effects

As explained by Njoku and Chan (2006), vegetation and surface roughness have similar effects on the observed brightness temperature (increases T_B and decreases the sensitivity to the surface emissivity to soil moisture), which makes it difficult to separate their impact. This statement applies to all the RTE-based vegetation parameterization approaches, such as those employed by NPD, LPRM and UMT.

The vegetation and roughness effects are described in the RTE through four parameters $h_{(f)}G$, $Q_{(f)}$, $\tau^c_{(f)}$ and $\omega_{(f)}$, where the impact of $Q_{(f)}$ and $\omega_{(f)}$ is linear, while $h_{(f)}$ and $\tau^c_{(f)}$ are exponentially related to the microwave signal. The general sensitivity of the RTE to each of these parameters individually is illustrated in Fig. 5 plot [a]. For example, 'bare/smooth' (blue line) shows the response over smooth bare soil conditions; the dark brown line in plot [a] shows the response from a bare rough surface, where the roughness parameterization is done by defining the $h_{(f)}$ parameter only, and so on. The synthetic runs shown in plot [a] of this figure were generated by varying only one parameter at a time and setting the remaining parameters to 0. The two options for G discussed earlier include $G = 1$ and $G = \cos^2\theta$. G has a direct impact on $\omega_{(f)}$. When expressed as a function of θ, G reduces the magnitude of $h(f)$ and therefore its impact on the sensitivity of the emissivity to *SM*. The difference between these two cases is small and becomes less important (and negligible) as $\tau_{(f)}{}^c$ increase. It can also be seen that parameterization of $Q_{(f)}$ and $\omega_{(f)}$ with any values different than 0 does not impact the sensitivity of the $e_{(10.7,H)}$–*SM* curve, respectively. This confirms the previous statement that the assumption of $\omega_{(f)} = 0$ is not essential and suggests that erroneous parameterization of $Q_{(f)}$ and $\omega_{(f)}$ may lead to errors in the final estimates, however, their impact on the soil moisture range is negligible (Van De Griend and Owe, 1994). Most importantly, Fig. 5 plot [a] shows that among all 4 parameters listed in the beginning of this paragraph $\tau^c_{(f)}$ is the single most important parameter that can cause a significant reduction in the sensitivity of the $e_{(10.7,\ H)}$–*SM* curve. As discussed in Section 3, $\tau^c_{(f)}$ is also the parameter that is parameterized using very different approaches by each algorithm (see Table 5).

At the satellite spatial footprint scale, however, the microwave signal emitted from a naturally varying ground surface can rarely be described by using only a single parameter. The emissivity response is the result of the complex interaction of $h_{(f)}G$, $Q_{(f)}$, $\tau^c_{(f)}$ and $\omega_{(f)}$. Even though $h_{(f)}G$ alone appears to have minimal impact, when combined together with the vegetation effects, it can further reduce the sensitivity of the estimated emissivity to soil moisture. Several general scenarios are illustrated in Fig. 5 plots [b]. Another observation that can be made from Fig. 5 plots [b] is that the sensitivity to soil moisture is lowest when defining all four vegetation and roughness related parameters ($h_{(f)}G(G = 1.0)$, $Q_{(f)}$, $\tau^c_{(f)}$ and $\omega_{(f)}$), which is an anticipated result and in line with the microwave theory. The only approach that parameterizes for all vegetation and roughness parameters is LPRM.

NPD and UMT assume that $\tau^c_{(f)}$ also incorporates roughness effects ($\tau^{c*}_{(f)}$; note that the NPD $\tau^{c*}_{(f)}$ corresponds to the $\beta\alpha g$ expression given in Eq. 16), which are parameterized independently by SCA and LPRM. The validity of the assumption that $\tau^c_{(f)}$ and $\tau^{c*}_{(f)}$ are comparable was explored and the results are displayed in Fig. 5 plot [c]. This appears to be a reasonable simplification, which may lead to some unaccounted residual roughness effects in the smooth emissivity response. The magnitude of this roughness related error is minimal and is a function of vegetation, soil moisture and $h_{(f)}$.

It was demonstrated that the impact of $\omega_{(f)}$ is minimal (Fig. 5 plot [a]) and that $\tau^c_{(f)} \approx \tau^{c*}_{(f)}$, which leads to the conclusion that the SCA and UMT modeled emissivity from a vegetated rough surface will be similar. It also means that they will be different as compared to the corresponding modeled estimate of LPRM. The NPD modeled response incorporates the combined effect of $Q_{(f)}$ and $\tau^{c*}_{(f)}$, suggesting different sensitivity than UMT and SCA. To some degree, this is counterintuitive as NPD and SCA employ similar assumptions and are based on the same simplified τ–ω model. In addition, as clarified by Njoku and Chan, 2006, the NPD model is calibrated to represent minimal roughness conditions, which are incorporated through the $Q_{(f)}$ factor (see Eq. 12).

The algorithm specific responses, generated using the exact values for $h_{(f)}G$, $Q_{(f)}$, $\tau_{(f)}{}^c$ and $\omega_{(f)}$ as defined by the developers and shown in Fig. 5 plot [d], confirm the above discussion. Note that plotted here is the A^* function, where $A^*{}_{(10.7,SM)} = [e_{(10.7,V)} - e_{(10.7,H)}]/[e_{(10.7,V)} + e_{(10.7,H)}]$ and $e_{(10.7,\ p)}$ represents the modeled emissivity from a vegetated rough surface (following the sensitivity example shown in Fig. 4 in

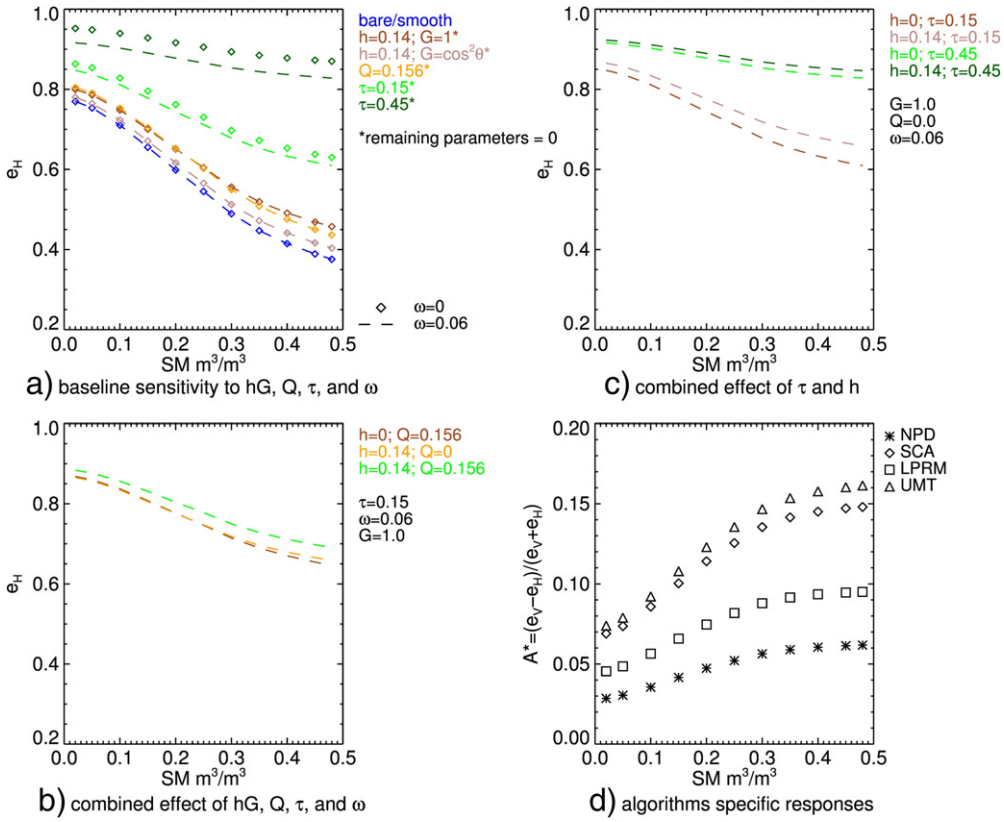

Fig. 5. RTE sensitivity analysis. All runs were done using the Wang and Schmugge dielectric mixing model applied for silt loam soils and using a constant effective temperature of 20 °C. Unless specified otherwise in the plot, with the exception of plot [d], runs were done using $h = 0.14$ and $Q = 0.156$ (average between the actual values adopted by the individual algorithms). The algorithms specific simulations, shown in plot [d], were done assuming fixed vegetation conditions ($\tau = 0.15$) and using the parameters listed in Table 5.

Njoku and Chan, 2006). Fig. 5 plot [d] shows that NPD, SCA, LPRM and UMT have different sensitivities. These results would also suggest that given the same $\tau^c_{(f)}$ parameterization, LPRM would have narrower range of soil moisture than SCA or UMT, which as seen from Fig. 3 is not the case. If we assume $\omega_{(f)} = 0$ and $Q_{(f)} = 0$, the LPRM emissivity approximation for smooth bare soil becomes equivalent to the SCA solution (Eq. 18). The vegetation–roughness exponential correction term for these two algorithms equals $e^{\left[h_{(f)}G+2\tau^c_{(f)}\right]}$. The corresponding functions for UMT and NPD equal $e^{\left[2\tau^c_{(f)}\right]}$ (Eq. 29, $\omega_{(f)} = 0$) and $e^{\left[b_1+b_2 \ln\left[MPDI^{dry}_{(f)}\right]\right]}$, respectively. Inter-comparing the full expression rather than focusing on $\tau^c_{(f)}$ alone allows examining the combined effect of $h_{(f)}G$ and $\tau^c_{(f)}$. The algorithm specific combined roughness–vegetation correction representations are shown in Fig. 6. All 4 maps display expected variability at global scale. However, the level of detail captured by each approach is slightly different. The few mountain areas present in the middle of Sahara and the Amazon River evident in the NPD, LPRM, and UMT maps, for example, are not distinguishable in the SCA map. The SCA $\tau^c_{(f)}$ parameterization is done using 10-day climatology, which can explain the different level of detail present in the SCA map. Agreement between the approaches is lower in the Northern latitudes. The most noticeable observation evident in this figure is the greater range of the LPRM exponential term. Even though SCA and LPRM correct in a similar way for the combined $h_{(f)}G$ and $\tau^c_{(f)}$ effect the absolute value of the corresponding exponential terms differs significantly between these two approaches. This difference is primarily controlled by $\tau^c_{(f)}$.

The analysis indicates that the characteristic soil moisture range of each retrieval algorithm is a function of the combined effect of the inherent algorithm specific sensitivity (Fig. 5) and the magnitude of the roughness–vegetation correction (Fig. 6). In the NPD case, the narrower range of soil moisture can be explained by the inherent minimal roughness effect and the fact that the algorithm models the current soil moisture as a deviation from some base line minimal vegetation and soil moisture conditions. As we saw from the sensitivity analysis presented in Fig. 5 the added roughness effect results in lower sensitivity as compared to the rest of the approaches. From any of the $R^{s,rough}_{(f,p)} \rightarrow R^{s,smooth}_{(f,p)}$ equations, it is easy to see that increased surface roughness would manifest as an increased soil emissivity and, as explained by Van De Griend and Owe (1994), this would result in a reduced wet–dry range in emissivity. Even though LPRM's sensitivity appears to be similar, its combined roughness–vegetation correction component is much higher leading to a different corrected emissivity and sensitivity of the $e^{s,smooth}_{(f,p)}$ to *SM*.

4.7. Detection of standing water

One additional factor that can alter the lower and upper end of the soil moisture range has to be considered. This is the impact of open water bodies and standing water. Algorithms, with the exception of UMT, screen for such unfavorable ground conditions using static ancillary maps, which only provide information on permanent features. Thus, it is very possible that areas experiencing temporary or short-term flooding will not be identified when using these databases. Standing water would result in underestimation of the effective soil emissivity, which in turn leads to overestimation of the soil moisture that produces a higher upper limit and larger range of soil moisture. Note that the presence of open water would contribute towards inaccuracies in both the soil emissivity and the effective temperature in approaches, where the latter is estimated using the higher frequencies of AMSR-E. If the observed difference in RANGE between LPRM and SCA and UMT were to be due to inaccurate screening for standing water, then these

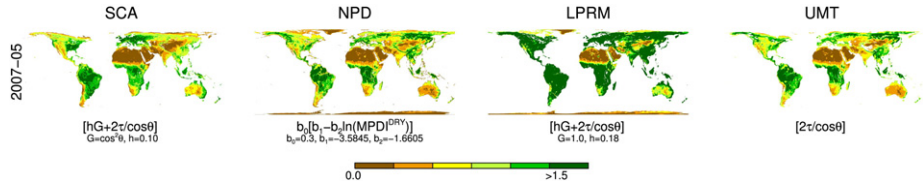

Fig. 6. An example of the vegetation–roughness correction term used by the individual algorithm, where each plot represents a monthly composite generated using data from May 2007. SCA approximates the vegetation contribution by utilizing an ancillary based approach, which relies on monthly NDVI climatology, while NPD, LPRM and UMT employ RTE modeling and microwave-based indices. Approaches show expected and comparable variability at global scale. The green spots located in the middle of Sahara, clearly evident in the NPD, LPRM and UMT maps, are major mountain features [Ahaggar, Tassili N'Ajjer (Algeria), Tibesti (Chad), and Aïr Mountains (Niger)]. These areas characterize with slightly wetter climate compared to the surrounding desert. The SCA maps display slightly lower level of detail (i.e. Sahara, Amazon River basin), which can be explained by the fact the SCA optical depth estimate is determined using climatology as opposed to real time data.

effects would be local and restricted to areas that are likely to experience occasional flooding. Such regional distributions are not evident in the RANGE maps (i.e. LPRM).

5. Concluding remarks

As stated in the Introduction, all passive microwave soil moisture retrieval approaches considered here are based on the same principles. However, the algorithms differ significantly in two ways: the simplifications of the RTE model employed and the approaches used for geophysical parameterization. It appears that the simplification of the RTE model based on the assumptions of $\omega_{(f)} = 0$, no atmospheric contribution and $\tau^{c}_{(f)} \approx \tau^{c*}_{(f)}$ is not significant. The more important difference in algorithm behavior arises from the inherent theoretical model sensitivity given the algorithm specific parameterization and the exponential correction component, which accounts for the combined $h_{(f)}G$ and $\tau^{c}_{(f)}$ contribution. The narrower soil moisture range observed in the NPD-based AMSR-E retrievals is a result of the inherent minimal roughness effect combined with the fact that the algorithm models the current soil moisture as a deviation from some base line minimal vegetation and soil moisture conditions. The temporal dynamics, on the other hand, is determined by the $MPDI_{(f)}$ response (see Eq. 15). Careful examination of the $MPDI_{(f)}$ response and how it relates to change in soil moisture conditions has to be conducted in order to determine how the temporal dynamics of the NPD product can be improved. In addition, several of the variables and constants used to compute Eqs. (15) and (16) were derived using a single year of AMSR-E observation (2003). Updating these parameters using the complete AMSR-E time period, would be a logical first next step towards enhancing the NPD product.

Although passive microwave-based soil moisture retrieval is considered a mature and reliable approach and the fact that several investigation have demonstrated the accuracy and sensitivity of some of the algorithms considered here (De Jeu et al., 2008; Draper et al., 2009; Jackson et al., 2010), our investigation has shown that each of the available approaches has shortcomings and inconsistencies:

- The LPRM optimization procedure minimizes the difference between observed and modeled $T^{t}_{B(f,p)}$ only for horizontal polarization; from a theoretical point of view this $T^{t}_{B(f,p)}$ includes information on the atmospheric water state, surface conditions, and soil moisture. Since $MPDI_{(f)}$ is used to approximate the vegetation effect, it might be more accurate if $MPDI_{(f)}$ was computed using the atmospherically corrected brightness temperature estimates and if the minimization was done simultaneously for both polarizations. It is likely that implementation of the above recommendations would require a more complex optimization procedure that is able to minimize multiple parameters simultaneously and an extra iteration loop to account for the atmospheric effect.
- SCA requires some ancillary data in order to estimate the vegetation contribution. Both UMT and NPD perform a double vegetation parameterization: UMT derives $\Gamma^{s}_{(f)}$ separately for the geophysical model and the soil moisture inversion. Similarly, the vegetation contribution in the NPD *SM* approach is done by evaluating the present $MPDI_{(f)}$ relative to the long term dry $MPDI_{(f)}$ at a single frequency (the operational vegetation-roughness parameter g is computed using two frequencies).

Most importantly, the sensitivity analysis presented in this paper leads towards the following general conclusions:

- Direct interchange of the final retrieved ancillary components is not recommended. This is especially true for parameters such as $\tau^{c}_{(f)}$, which do not have a directly observable geophysical equivalent that can be used for validation. Cross-comparisons against alternative vegetation-based data sets provide information on their relative performance in terms of spatial and temporal variability. However, they cannot access their accuracy in terms of physical range and absolute value.
- There is no 'perfect' parameterization approach. Algorithms are a system of interconnected units, where the retrieval of each geophysical parameter is done sequentially. This complicates the interchange of parameterization units between approaches. The RTE-based geophysical retrieval approaches are only possible if solved in an iterative optimization framework, which makes the solutions not easily transferable (i.e. inverse vs. forward solutions). Most importantly, as it was demonstrated, all of these parameterization units are complimentary to one another, which allow compensating for offsets in any of the units and balancing the system. That is to say that a 'combined RTE solution' that includes the 'best' features of each algorithm might be the most desirable and logical approach towards the establishment of the 'perfect' soil moisture model. However, it will not be an easily accomplishable task.

Theoretically each of the algorithms discussed in our paper can be applied to any system that operates at $f \leq 11$ GHz, including L-band, which is considered optimal for soil moisture monitoring. Since the assumptions and simplifications made by the algorithms remain valid at $f \leq 11$ GHz using an alternative frequency (i.e. L-, C- or X-band) will not have any impact on the algorithms' specific solutions. The intercomparisons offered in this paper will hopefully contribute to a better understating of the theoretical aspects that determine the sensitivity and overall performance of each algorithm. Such knowledge is essential as it provides a basis for improvement and can be beneficial for any future implementations of the algorithms examined here using alternative frequency ($f \leq 11$ GHz) or observations acquired from a different microwave system.

To reiterate a statement made earlier, the discussion and analysis presented in this paper do not reflect on the statistical accuracy of the available products, we did not perform an evaluation of the accuracy of the soil moisture retrievals. Goals were to determine the cause(s) for the different range of the soil moisture estimates and temporal dynamics displayed by the alternative approaches and potentially outline the components from the NPD algorithm that would need to be modified or improved. In this paper it was assumed that differences caused by the dielectric mixing model (i.e. Dobson vs. Wang and Schmugge) and the ancillary static data sets (i.e. soil properties) are minimal as compared to deviations caused by the algorithm specific RTE parameters. Therefore, an important supplementary analysis would be to assess

the total error associated with the assumptions, use of spatially fixed soil properties, use of static dataset for detection of dynamic variables such as standing water, etc. Careful assessment of these intrinsic errors in addition to the relative accuracy of the final products is essential and would potentially lead to better understanding of the advantages and shortcomings of the available approaches.

References

Atkinson, P. M., & Tatnall, A. R. L. (1997). Introduction neural networks in remote sensing. *International Journal of Remote Sensing*, *18*(4), 699–709. http://dx.doi.org/10.1080/014311697218700.

Bolten, J. D., Crow, W. T., Zhan, X., Jackson, T. J., & Reynolds, C. A. (2010). Evaluating the utility of remotely sensed soil moisture retrievals for operational agricultural drought monitoring. *IEEE Journal of Selected Topics in Applied Earth Observations and Remote Sensing*, *3*(1), 57–66. http://dx.doi.org/10.1109/JSTARS.2009.2037163.

Choudhury, B. J., Schmugge, T. J., Chang, A., & Newton, R. W. (1979). Effect of surface roughness on the microwave emission from soils. *Journal of Geophysical Research*, *84*, 5699–5706.

Colwell, R. N., Simonett, D. S., & Ulaby, F. T. (Eds.). (1983). *Manual of remote sensing. Theory, instruments and techniques, vol. I*, Falls Church.

Crow, W. T., Miralles, D. G., & Cosh, M. H. (2010). A quasi-global evaluation system for satellite surface soil moisture retrievals. *IEEE Transactions on Geoscience and Remote Sensing*, *48*(6), 2516–2527.

De Jeu, R. A. M., & Owe, M. (2003). Further validation of a new methodology for surface moisture and vegetation optical depth retrieval. *International Journal of Remote Sensing*, *24*(22), 4559–4578.

De Jeu, R. A. M., Wagner, W., Holmes, T. R. H., Dolman, A. J., Van De Giesen, N. C., & Friesen, J. (2008). Global soil moisture patterns observed by space borne microwave radiometers and scatterometers. *Surveys in Geophysics*, *29*(4), 399–420.

Dobson, M. C., Ulaby, F. T., Hallikainen, M. T., & El-Rayes, M. A. (1985). Microwave dielectric behavior of wet soil — Part II: Dielectric mixing models. *IEEE Transactions on Geoscience and Remote Sensing*, *23*(1), 35–46.

Draper, C. S., Walker, J. P., Steinle, P. J., De Jeu, R. A. M., & Holmes, T. R. H. (2009). An evaluation of AMSR-E derived soil moisture over Australia. *Remote Sensing of Environment*, *113*(4), 703–710. http://dx.doi.org/10.1016/j.rse.2008.11.011.

Drusch, M. (2007). Initializing numerical weather prediction models with satellite derived surface soil moisture: Data assimilation experiments with ECMWF's integrated forecast system and the TMI soil moisture data set. *Journal of Geophysical Research*, *112*, D03102. http://dx.doi.org/10.1029/2006JD007478.

Entekhabi, D., Njoku, E. G., O'Neill, P. E., Kellogg, K. H., Crow, W. T., Edelstein, W. N., et al. (2010). The soil moisture active passive (SMAP) mission. *Proceedings of the IEEE*, *98*(5), 704–716.

Ferrazzoli, P., Paloscia, S., Pampaloni, P., Schiavon, G., Solimini, D., & Coppo, P. (1992). Sensitivity to microwave measurements to vegetation biomass and soil moisture content: A case study. *IEEE Transactions on Geoscience and Remote Sensing*, *30*(4), 750–756. http://dx.doi.org/10.1109/36.158869.

Hallikainen, M. T., Ulaby, F. T., Dobson, M. C., El-Rayes, M. A., & Wu, L. -K. (1985). Microwave dielectric behavior of wet soil—Part 1: Empirical models and experimental observations. *IEEE Transactions on Geoscience and Remote Sensing*, *GE-23*(1), 25–34. http://dx.doi.org/10.1109/TGRS.1985.289497.

Holmes, T. R. H., De Jeu, R. A. M., Owe, M., & Dolman, A. J. (2009). Land surface temperature from Ka band (37 GHz) passive microwave observations. *Journal of Geophysical Research*, *114*(D4), D04113. http://dx.doi.org/10.1029/2008JD010257.

Holmes, T. R. H., Jackson, T. J., Reichle, R. H., & Basara, J. B. (2014). An assessment of surface soil temperature products from numerical weather prediction models using ground-based measurements. *Water Resources Research*, *48*(2). http://dx.doi.org/10.1029/2011WR010538 (W02531).

Hornik, K., Stinchcombe, M., & White, H. (1989). Multilayer feedforward networks are universal approximators. *Neural Networks*, *2*(5), 359–366. http://dx.doi.org/10.1016/0893-6080(89)90020-8.

Imaoka, K., Kachi, M., Fujii, H., Murakami, H., Hori, M., Ono, A., et al. (2010). Global change observation mission (GCOM) for monitoring carbon, water cycles, and climate change. *Proceedings of the IEEE*, *98*(5), 717–734. http://dx.doi.org/10.1109/JPROC.2009.2036869.

Jackson, T. J. (1993). Measuring surface soil moisture using passive microwave remote sensing. *Hydrological Processes*, *7*, 139–152.

Jackson, T. J., Cosh, M. H., Bindlish, R., Starks, P. J., Bosch, D., Seyfried, M., et al. (2010). Validation of advanced microwave scanning radiometer soil moisture products. *IEEE Transactions on Geoscience and Remote Sensing*, *48*(12), 4256–4272.

Jackson, T. J., Hsu, A. Y., Van De Griend, A. A., & Eagleman, J. R. (2004). Skylab L-band microwave radiometer observations of soil moisture revisited. *International Journal of Remote Sensing*, *25*(13), 2585–2606.

Jackson, T. J., Le Vine, D. M., Hsu, A. Y., Oldack, A., Starks, P. J., Swift, C. T., et al. (1999). Soil moisture mapping at regional scales using microwave radiometry: The Southern Great Plains Hydrology Experiment. *IEEE Transactions on Geoscience and Remote Sensing*, *37*, 2136–2149.

Jackson, T. J., & Schmugge, T. J. (1989). *Algorithm for the passive microwave remote sensing of soil moisture, in Microwave Radiometry and Remote Sensing Applications, Utrecht, the Netherlands.*

Jackson, T. J., & O'Neill, P. E. (1991). Microwave emission and crop residues. *Remote Sensing of Environment*, *36*(2), 129–136. http://dx.doi.org/10.1016/0034-4257(91)90035-5.

Jackson, T. J., & Schmugge, T. J. (1991). Vegetation effects on the microwave emission of soils. *Remote Sensing of Environment*, *36*(3), 203–212.

Jackson, T. J., Schmugge, T. J., & Wang, J. R. (1982). Passive microwave sensing of soil moisture under vegetation canopies. *Water Resources Research*, *18*(4), 1137–1142.

Jones, L. A., Ferguson, C. R., Kimball, J. S., Zhang, K., Chan, S. T. K., McDonald, K. C., et al. (2010). Satellite microwave remote sensing of daily land surface air temperature minima and maxima from AMSR-E. *IEEE Journal of Selected Topics in Applied Earth Observations and Remote Sensing*, *3*(1), 111–123. http://dx.doi.org/10.1109/JSTARS.2010.2041530.

Jones, M. O., Jones, L. A., Kimball, J. S., & McDonald, K. C. (2011). Satellite passive microwave remote sensing for monitoring global land surface phenology. *Remote Sensing of Environment*, *115*(4), 1102–1114. http://dx.doi.org/10.1016/j.rse.2010.12.015.

Jones, L. A., Kimball, J. S., Podest, E., McDonald, K. C., Chan, S. K., & Njoku, E. G. (2009). A method for deriving land surface moisture, vegetation optical depth, and open water fraction from AMSR-E. *Geoscience and Remote Sensing Symposium, 2009 IEEE International, IGARSS 2009*, *3*. (pp. III-916–III-919). http://dx.doi.org/10.1109/IGARSS.2009.5417921.

Kawanishi, T., Sezai, T., Ito, Y., Imaoka, K., Takeshima, T., Ishido, Y., et al. (2003). The Advanced Microwave Scanning Radiometer for the Earth Observing System (AMSR-E), NASDA's contribution to the EOS for global energy and water cycle studies. *IEEE Transactions on Geoscience and Remote Sensing*, *41*(2), 184–194.

Kerr, Y. H., & Njoku, E. G. (1990). A semiempirical model for interpreting microwave emission from semiarid land surfaces as seen from space. *IEEE Transactions on Geoscience and Remote Sensing*, *28*(3), 384–393.

Kerr, Y. H., Waldteufel, P., Richaume, P., Wigneron, J. P., Ferrazzoli, P., Mahmoodi, A., et al. (2012). The SMOS soil moisture retrieval algorithm. *IEEE Transactions on Geoscience and Remote Sensing*, *50*(5), 1384–1403. http://dx.doi.org/10.1109/TGRS.2012.2184548.

Kirdiashev, K. P., Chukhlantsev, A. A., & Shutko, A. M. (1979). Microwave radiation of the earth's surface in the presence of vegetation cover. *Radiotekhnika I Elektronika*, *24*, 256–264.

Klein, L. A., & Swift, C. T. (1977). An improved model for the dielectric constant of sea water at microwave frequencies. *IEEE Transactions on Antennas and Propagation*, *AP-25*(1), 104–111.

Koike, T., Nakamura, Y., Kaihotsu, I., Davva, G., Matsuura, N., Tamagawa, K., et al. (2004). Development of an Advanced Microwave Scanning Radiometer (AMSR-E) algorithm of soil moisture and vegetation water content. *Annual Journal of Hydraulic Engineering, JSCE*, *48*, 217–222.

Koster, R. D., Guo, Z., Yang, R., Dirmeyer, P. A., Mitchell, K., & Puma, M. J. (2009). On the nature of soil moisture in land surface models. *Journal of Climate*, *22*(16), 4322–4335. http://dx.doi.org/10.1175/2009JCLI2832.1.

Lee, S. L. (1974). Dual frequency microwave radiometer measurements of soil moisture for bare and vegetated rough surfaces. http://ntrs.nasa.gov/search.jsp?R=19740026660

Lek, S., Delacoste, M., Baran, P., Dimopoulos, I., Lauga, J., & Aulagnier, S. (1996). Application of neural networks to modelling nonlinear relationships in ecology. *Ecological Modelling*, *90*(1), 39–52. http://dx.doi.org/10.1016/0304-3800(95)00142-5.

Li, L., Gaiser, P. W., Gao, B. C., Bevilacqua, R. M., Jackson, T. J., Njoku, E. G., et al. (2010). WindSat global soil moisture retrieval and validation. *IEEE Transactions on Geoscience and Remote Sensing*, *48*(5), 2224–2241.

Lu, H., Koike, T., Fujii, H., Ohta, T., & Tamagawa, K. (2009). Development of a physically-based soil moisture retrieval algorithm for spaceborne passive microwave radiometers and its application to AMSR-E. *Journal of the Remote Sensing Society of Japan*, *29* (http://agris.fao.org/agris-search/search/display.do?f=2009/JP/JP0923.xml;JP2009003143).

Mas, J. F., & Flores, J. J. (2008). The application of artificial neural networks to the analysis of remotely sensed data. *International Journal of Remote Sensing*, *29*(3), 617–663. http://dx.doi.org/10.1080/01431160701352154.

Meesters, A. G. C. A., De Jeu, R. A. M., & Owe, M. (2005). Analytical derivation of the vegetation optical depth from the microwave polarization difference index. *IEEE Geoscience and Remote Sensing Letters*, *2*(2), 121–123.

Mo, T., Choudhury, B. J., Schmugge, T. J., Wang, J. R., & Jackson, T. J. (1982). A model for microwave emission from vegetation-covered fields. *Journal of Geophysical Research*, *87*(C13), 11229–11237. http://dx.doi.org/10.1029/JC087iC13p11229.

Mo, T., & Schmugge, T. J. (1987). A parameterization of the effect of surface roughness on microwave emission. *IEEE Transactions on Geoscience and Remote Sensing*, *25*(4), 481–486. http://dx.doi.org/10.1109/TGRS.1987.289860.

Njoku, E. G., & Chan, S. K. (2006). Vegetation and surface roughness effects on AMSR-E land observations. *Remote Sensing of Environment*, *100*(2), 190–199.

Njoku, E., Chan, T., Crosson, W., & Limaye, A. (2004). Evaluation of the AMSR-E data calibration over land. *Italian Rournal of Remote Sensing*, *30/31*, 19–37.

Njoku, E. G., Jackson, T. J., Lakshmi, V., Chan, T. K., & Nghiem, S. V. (2003). Soil moisture retrieval from AMSR-E. *IEEE Transactions on Geoscience and Remote Sensing*, *41*, 215–229.

Njoku, E. G., & Li, L. (1999). Retrieval of land surface parameters using passive microwave measurements at 6–18 GHz. *IEEE Transactions on Geoscience and Remote Sensing*, *37*(1), 79–93.

Oki, T., Imaoka, K., & Kachi, M. (2010). AMSR instruments on GCOM-W1/2: Concepts and applications. *Geoscience and remote sensing symposium (IGARSS), 2010 IEEE International* (pp. 1363–1366). http://dx.doi.org/10.1109/IGARSS.2010.5650001.

Owe, M., De Jeu, R., & Holmes, T. (2008). Multisensor historical climatology of satellite-derived global land surface moisture. *Journal of Geophysical Research*, *113*(F01002), 17. http://dx.doi.org/10.1029/2007JF000769.

Owe, M., De Jeu, R. A. M., & Walker, J. P. (2001). A methodology for surface soil moisture and vegetation optical depth retrieval using the microwave polarization

difference index. *IEEE Transactions on Geoscience and Remote Sensing*, *39*(8), 1643–1654.

Paloscia, S., Macelloni, G., & Santi, E. (2006). Soil moisture estimates from AMSR-E brightness temperatures by using a dual-frequency algorithm. *IEEE Transactions on Geoscience and Remote Sensing*, *44*(11), 3135–3144.

Paloscia, S., Macelloni, G., Santi, E., & Koike, T. (2001). A multifrequency algorithm for the retrieval of soil moisture on a large scale using microwave data from SMMR and SSM/I satellites. *IEEE Transactions on Geoscience and Remote Sensing*, *39*(8), 1655–1661.

Paloscia, S., Pampaloni, P., Chiarantini, L., Coppo, P., Gagliani, S., & Luzi, G. (1993). Multifrequency passive microwave remote sensing of soil moisture and roughness. *International Journal of Remote Sensing*, *14*(3), 467–483. http://dx.doi.org/10.1080/01431169308904351.

Parinussa, R. M., Holmes, T. R. H., Yilmaz, M. T., & Crow, W. T. (2011). The impact of land surface temperature on soil moisture anomaly detection from passive microwave observations. *Hydrology and Earth System Sciences*, *15*(10), 3135–3151. http://dx.doi.org/10.5194/hess-15-3135-2011.

Pellarin, T., Wigneron, J. -P., Calvet, J. -C., Berger, M., Douville, H., Ferrazzoli, P., et al. (2003). Two-year global simulation of L-band brightness temperatures over land. *IEEE Transactions on Geoscience and Remote Sensing*, *41*(9–2), 2135–2139.

Poe, G. A., & Edgerton, A. T. (1971). *Determination of soil moisture content with airborne microwave radiometry.*

Qiu, Y., Shi, J., Jiang, L., & Mao, K. (2007). Study of atmospheric effects on AMSR-E microwave brightness temperature over Tibetan Plateau. *Geoscience and remote sensing symposium, 2007. IGARSS 2007. IEEE International* (pp. 1873–1876). http://dx.doi.org/10.1109/IGARSS.2007.4423189.

Reichle, R. H., Koster, R. D., Dong, J., & Berg, A. A. (2004). Global soil moisture from satellite observations, land surface models, and ground data: Implications for data assimilation. *Journal of Hydrometeorology*, *5*(3), 430–442. http://dx.doi.org/10.1175/1525-7541(2004) 005<0430:GSMFSO>2.0.CO;2.

Reynolds, C. A., Jackson, T. J., & Rawls, W. J. (2000). Estimating soil water-holding capacities by linking the Food and Agriculture Organization soil map of the world with global pedon databases and continuous pedotransfer functions. *Water Resources Research*, *36*(12), 3653–3662. http://dx.doi.org/10.1029/2000WR900130.

Santi, E. (2010). An application of SFIM technique to enhance the spatial resolution of microwave radiometers. *International Journal of Remote Sensing*, *31*, 2419–2428.

Santi, E., Pettinato, S., Paloscia, S., Pampaloni, P., Macelloni, G., & Brogioni, M. (2012). An algorithm for generating soil moisture and snow depth maps from microwave spaceborne radiometers: Hydroalgo. *Hydrology and Earth System Sciences Discussions*, *9*(3), 3851–3900. http://dx.doi.org/10.5194/hessd-9-3851-2012.

Schmugge, T. (1980). Soil moisture sensing with microwave radiometers. http://docs.lib.purdue.edu/lars_symp/392/

Sharkov, E. A. (2003). Passive microwave remote sensing of the earth: Physical foundations. : Springer.

Shibata, A., Imaoka, K., & Koike, T. (2003). AMSR/AMSR-E level 2 and 3 algorithm developments and data validation plans of NASDA. *IEEE Transactions on Geoscience and Remote Sensing*, *41*(2), 195–203. http://dx.doi.org/10.1109/TGRS.2002.808320.

Stogryn, A. (1970). The brightness temperature of a vertically structured medium. *Radio Science*, *5*(12), 1397–1406. http://dx.doi.org/10.1029/RS005i012p01397.

Ulaby, F. T., Moore, R. K., & Fung, A. K. (Eds.). (1981). *Microwave remote sensing: Active and passive. Microwave remote sensing fundamentals and radiometry, vol. I*, Reading, Massachusetts: Addison-Wesley.

Ulaby, F. T., Moore, R. K., & Fung, A. K. (1986). Microwave remote sensing: Active and passive. *From theory to applications, vol. III*, Norwood, MA: Artech House.

Ulaby, F. T., & Wilson, E. A. (1985). Microwave attenuation properties of vegetation canopies. *IEEE Transactions on Geoscience and Remote Sensing*, *GE-23*(5), 746–753. http://dx.doi.org/10.1109/TGRS.1985.289393.

Van De Griend, A. A., & Owe, M. (1994). Microwave vegetation optical depth and signal scattering albedo from large scale soil moisture and NIMBUS/SMMR satellite observations. *Meteorology and Atmospheric Physics*, *54*, 225–239.

Van De Griend, A. A., & Wigneron, J. P. (2004). On the measurement of microwave vegetation properties: Some guidelines for a protocol. *IEEE Transactions on Geoscience and Remote Sensing*, *42*(10), 2277–2289. http://dx.doi.org/10.1109/TGRS.2004.832243.

Wang, J. R., & Choudhury, B. J. (1981). Remote sensing of soil moisture content over bare field at 1.4 GHz frequency. *Journal of Geophysical Research*, *86*(C6), 5277–5287.

Wang, J. R., & Choudhury, B. J. (1995). Passive microwave radiation from soil: Examples of emission models and observations. In B. J. Choudhury, Y. H. Kerr, E. G. Njoku, & P. Pampaloni (Eds.), *Passive microwave remote sensing of land–atmosphere interactions*. Utrecht: VSP Publishing.

Wang, J. R., Mcmurtrey, J. E., III, Engman, E. T., Jackson, T. J., Schmugge, T. J., Gould, W. I., et al. (1982). Radiometric measurements over bare and vegetated fields at 1.4-GHz and 5-GHz frequencies. *Remote Sensing of Environment*, *12*(4), 295–311.

Wang, J. R., O'Neill, P. E., Jackson, T. J., & Engman, E. T. (1983). Multifrequency measurements of the effects of soil moisture, soil texture, and surface roughness. *IEEE Transactions on Geoscience and Remote Sensing*, *1*, 44–51.

Wang, J. R., & Schmugge, T. J. (1980). An empirical model for the complex dielectric permittivity of soils as a function of water content. *IEEE Transactions on Geoscience and Remote Sensing*, *18*(4), 288–295.

Wentz, F. J., Gentemann, C., Smith, D., & Chelton, D. B. (2000). Satellite measurements of sea surface temperature through clouds. *Science*, *288*(5467), 847–850. http://dx.doi.org/10.1126/science.288.5467.847.

Wilheit, T. T. (1978). Radiative transfer in a plane stratified dielectric. *IEEE Transactions on Geoscience Electronics*, *16*(2), 138–143.